ASYMMETRICAL I-V CURVES FROM A SYMMETRICAL DEVICES STRUCTURE OF ORGANIC PHOTOVOLTAICS

ASYMMETRICAL I-V CURVES FROM A SYMMETRICAL DEVICES STRUCTURE OF ORGANIC PHOTOVOLTAICS

By

SHANGZHI CHEN, B.Eng.

A Thesis

Submitted to the school of Graduate Studies

In Partial Fulfillment of the Requirements

For the Degree

Master of Applied Science

McMaster University

MASTER OF APPLIED SCIENCE (2013)   McMaster University

(Materials Science & Engineering)   Hamilton, Ontario

TITLE: Asymmetrical I-V curves from a symmetrical devices structure of

Organic Photovoltaics

AUTHOR: Shangzhi Chen, B. Eng. (Shanghai Jiao Tong University)

SUPERVISOR: Professor Gu Xu

NUMBER OF PAGES: XII, 84

Abstract

The energy diagram for organic photovoltaics (OPV), involving the bulk heterojunction (BHJ), on which the device analysis is usually based, has long been a subject of debate. The widely used Metal-insulator-Metal model and P-type Schottky Junction model, both of which are based on inappropriate assumptions, could be incorrect to explain the working principle of BHJ OPV.

To further explore the controversy, we start the investigation from the opposite direction, to the usually asymmetrical OPV, involving electron and hole passages, by introducing a pair of symmetric electrodes to a BHJ, to form a completely symmetrical device structure, which, in theory, would produce zero output.

Surprisingly, it is found that such a symmetrical device exhibits asymmetrical I-V curves. In particular, it produces a non-zero open-circuit voltage, and a finite short-circuit current. The cause of the output was the asymmetrical charge carrier distribution due to the asymmetrical illumination. To explain the operational mechanism of the symmetrical device, the equivalent circuit including a pair of inverse-parallel diodes and a new model for the BHJ energy diagram are introduced. Those findings would certainly improve the understanding of the device physics of OPV, especially the working principle for BHJ.

Acknowledgement

First of all, I would like to sincerely appreciate and thank my supervisor Prof. Gu Xu for providing me the opportunity to explore in the field of organic photovoltaics. I also thank for his patient guidance, inspiring encouragement, and invaluable discussions.

I appreciate the help from my colleagues and all the friends who motivated and supported me during my study. I thank Dr. Cindy X. Zhao, Dr. Han Yan, Lucy L. Deng, Matthew Y. Ma, Alice Y. Mao, and Renee W. Li for their consistent support during my entire graduate career.

I also thank Professors who instructed the courses that I attended through these two years. The knowledge I learned from those courses does help me a lot. I do sincerely appreciate all the staffs in our MSE department.

Finally, I devote my heartiest appreciation to my parents and my grandparents for their love and affection that inspired me throughout my life.

Table of Contents

List of Figures

x

List of Tables

Chapter 1 Introduction

1.1 Renewable energy and photovoltaics

Fossil fuels, including coal, petroleum, and natural gas, are resources derived from natural processes such as anaerobic decomposition of buried dead organisms. Mostly, the fulfillment of such processes may cost millions of years and render the fossil fuels as non-renewable energy resources. The carbon dioxide emitted by combustion of fossil fuels is called greenhouse gas, which is considered as an important cause of the global warming and anthropogenic climate change. According to the World Energy Review in June 2013[1], the annual global energy consumption grows at a speed of 2.6% for the last ten years. About 81% of world's energy is provided by those fossil fuels up to now, while the reserves of them are expected to be significantly exhausted by the end of this century. [2] The search for environmentally clean and renewable energy alternatives to supplement and replace the depleting fossil fuels is still under continual investigation.

1.1.1 Renewable energy

To distinguish with the fossil fuels, the energy formed by the natural processes that are replenished constantly is defined as Renewable Energy. The wind, hydropower, tidal, geothermal, biomass, and solar energy are the most common forms of renewable energy (**Figure** 1.1). Most types of renewable energy derive their energy from the sun directly or indirectly.
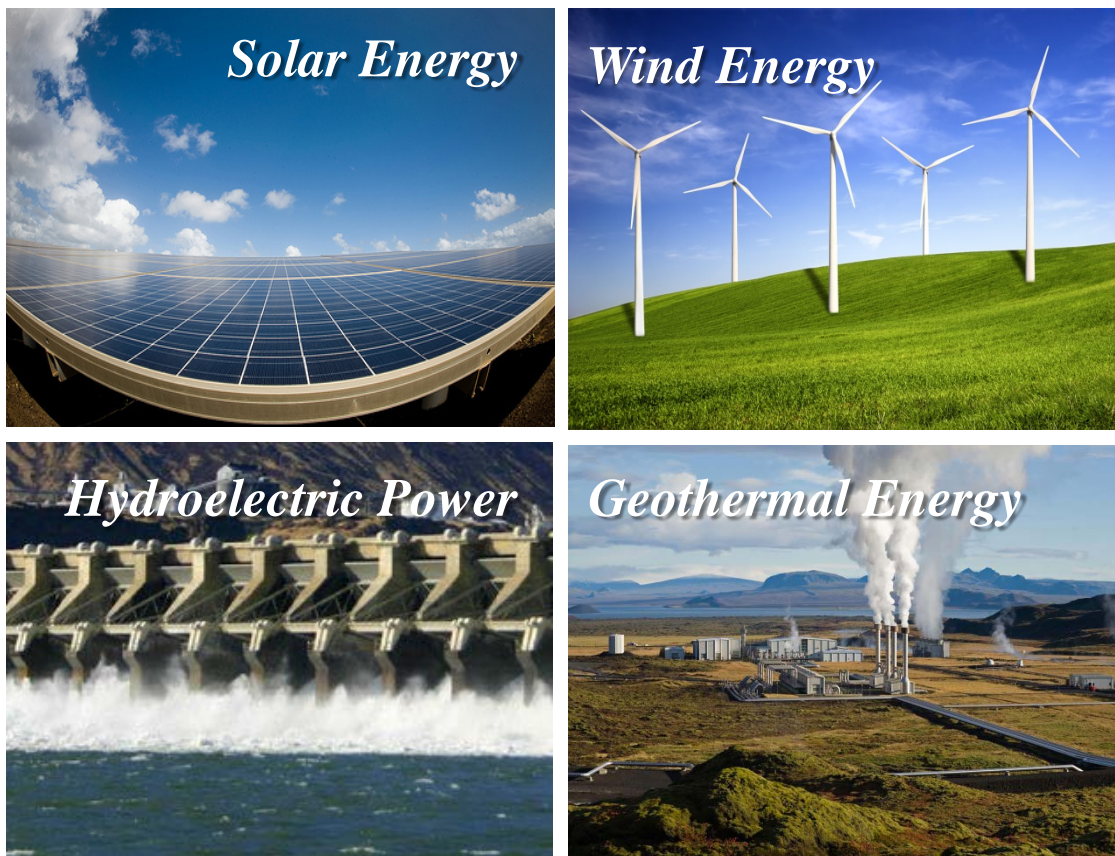
Figure 1.1 The renewable energy [3-6]

Lots of attempts in renewable energy application have been made to satisfy the

increasing global energy demand, such as wind farm, and Geothermal Power Station. Although the renewable energy is largely developed currently, they are not yet cost-effective enough for a replacement. As depicted in **Figure** 1.2, the share of renewable energy in the Global energy consumption is only 16%.
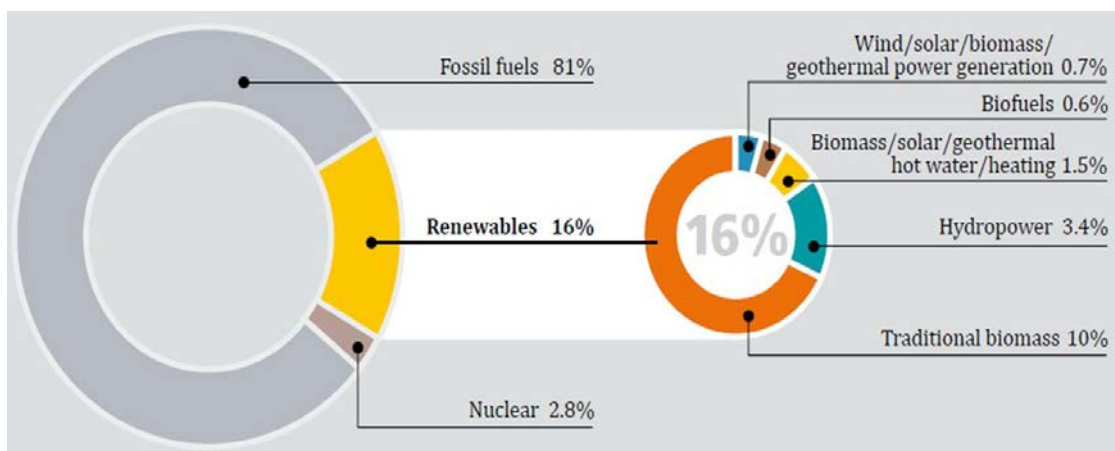
Figure 1.2 Renewable energy as share of annual world

Energy consumption in 2011 [7]

1.1.2 Solar energy

Considered as the most promising candidate, the solar energy is the most abundant, inexhaustible, and cleanest renewable energy available. Sunlight is a mixture of electromagnetic waves comprised of infrared, visible, and ultraviolet light. The solar spectrum, which is similar to that of a 5800 K black body, is displayed in **Figure** 1.3. The total energy emitted from the Sun that strikes the face of the Earth is

5.5×10^{24} joules per year, which is more than the annual total energy consumption of the world (5.0×10^{20} joules for 2010). [8] For a single day, the sun supplies the earth surface with a radiant energy of about 1.5×10^{22} J, which is enough to accommodate the needs for all the earth's inhabitants for at least 30 years.

Solar Radiation Spectrum
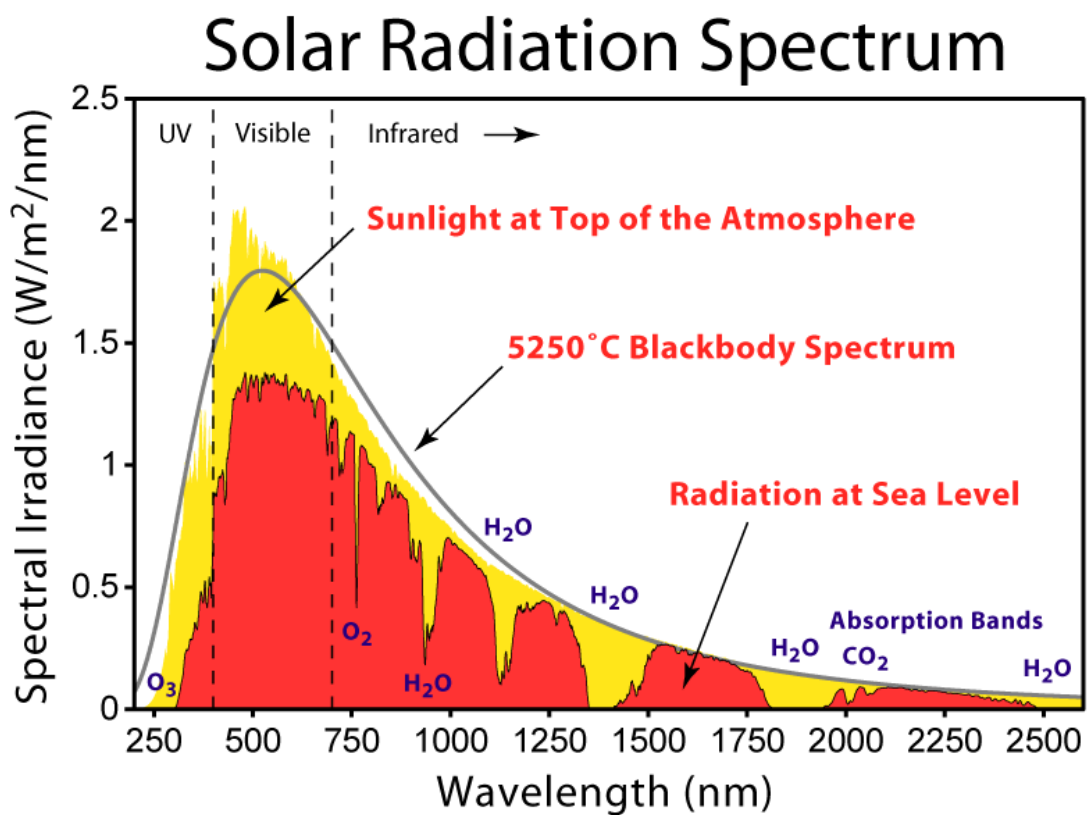
Figure 1.3 The solar spectrum [9]

The effective solar energy application systems convert the sun's light or heat to various forms of energy we need. The human beings have a long history in exploration of solar energy. As early as 2nd century BC, the Greek physicist Archimedes already

acquired the technology of solar heating and once used it to destroy the enemy ships with fire. [10]

Solar thermal and photovoltaics are two basic ways for the conversion. There are two types of solar thermal system: passive and active. No facility is required for the passive system. For instance, the temperature increase in a car parked in the sun is a passive system. The active system usually needs a thermal collector to take the sun's ray, such as the Solar Water Heating (SWH) system. A lot of solar thermal applications are exploited in both public and commercial entities. By running a heat engine, the captured solar heat could also produce electricity. However, this is different from the direct solar energy to electricity conversion in Photovoltaic technology.

1.2 A brief history of solar cells

Photovoltaic cell, or solar cell, is the electronic device that converts the solar energy into electricity based on the photovoltaic effect, which was first discovered by a French physicist A. E. Becquerel in 1839. [11] According to Becquerel's research, platinum electrodes coated by light-sensitive materials (silver chloride, AgCl) immersed in the acidic solution could provide finite output current and voltage under illumination. The solid state solar cell, however, didn't emerge until forty-four years later when C. Fritts made a junction device between thin gold layer and semiconductor

selenium (Se) with an efficiency of about 1%. [12] In 1888, A. Stoletov invented the photoelectric cell [13] by employing the photoelectric effect which brought A. Einstein a Nobel Prize in Physics [14].
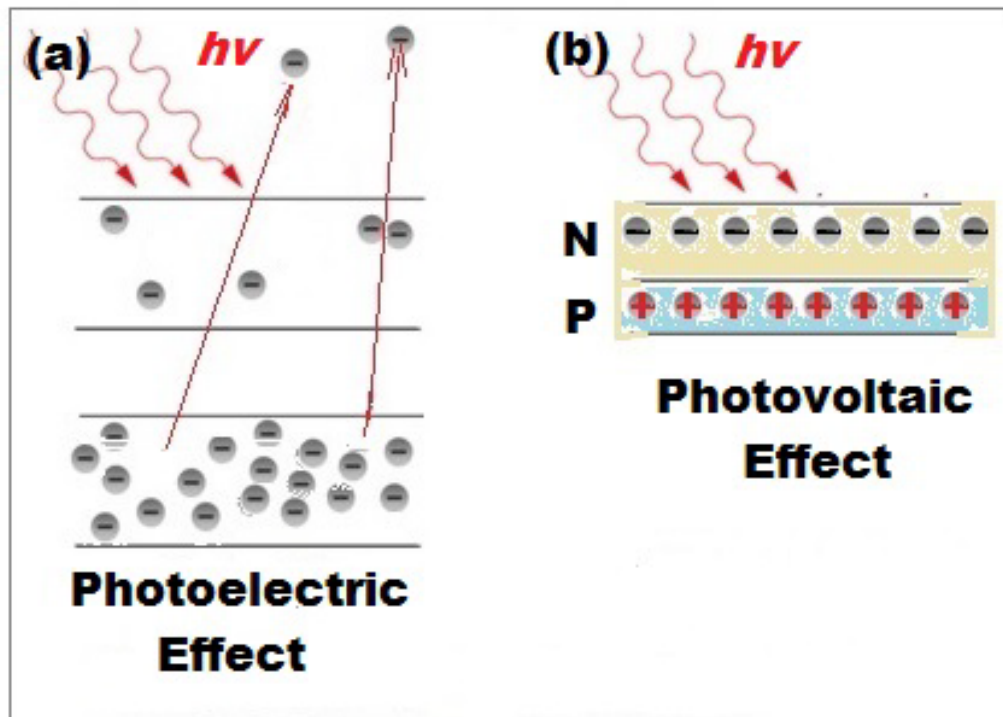
Figure 1.4 The photoelectric effect (a) and the photovoltaic effect (b)

Since sharing lots of common features, the photovoltaic effect is easily confused with the photoelectric effect. The illustrated diagrams (**Figure** 1.4) are used to clarify the difference between them. In the photoelectric effect, the electrons are ejected from a material's surface and passing through the vacuum to reach another

material under illumination. However, upon exposure to light, the excited electrons would jump from the valence band to the conduction band and be transported to a different material directly by an internal electric filed in the photovoltaic effect.

The p/n junction, which was first witnessed by R. S. Ohl in 1939 [15], broadens the photovoltaic research horizontals and makes the commercialization of the inorganic solar cell possible. In 1946, inspired by the diodes researches, Ohl invented the modern junction semiconductor (silicon) solar cell prototype and patented it as "Light sensitive device" [16].
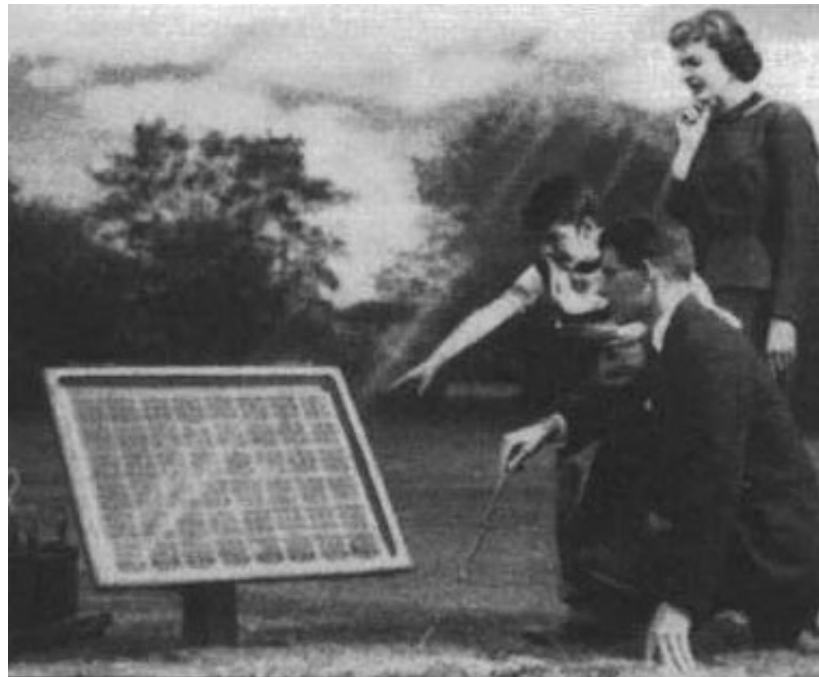
Figure 1.5 The first practical solar cell [19]

The first practical inorganic solar cell (**Figure** 1.5) with an efficiency of 6% was invented by D. Chapin, C. Fuller, and G. Pearson at Bell Laboratories in 1954. [17] And further enhancement made by L. Hoffman improved the efficiency from 2% to 14% for the large scale production. [18] However, the high cost ($250 per watt) caused by the raw material made it less competitive, especially in comparison with the fossil fuels ($2 per watt).

In order to reduce the cost of raw materials, other inorganic semiconductor materials are under active investigation, such as amorphous silicon (α-Si), cadmium telluride (CdTe), copper indium gallium diselenide (CIGS). Those semiconductors are applied in the form of thin films with thickness of several micrometers. The solar cells made of these are usually called the second generation solar cell (or thin-film solar cell), while the first generation is defined as the devices mainly use crystalline silicon as raw materials.

Those new semiconductors provide a better solar absorption, a lower fabrication cost, and a much easier procedures. Both CdTe (16.5%) [20] and CIGS (19.2%) [21] thin film solar cells exhibited high efficiencies in the lab. First Solar, Inc. is the largest manufacturer and seller of thin film solar panel in the world and they successfully reduced the cost below $1.00 per watt by using CdTe as raw material. [22] The second generation solar cells are accountable for 16.8% shares of solar panel market in 2009. [23] However, the problems found in the mass production such as the

toxicity (cadmium and lead), the stability (α-Si) of the thin film largely restrict the further development.

The 1990s should be the golden age of solar cell researches. Aside from the monocrystalline silicon solar cell with an efficiency of 24.4% was fabricated (1998) [24], great achievements were made by the introduction of new concept and emerging technology. The nanostructured solar cell (NSC), the dye-sensitized solar cell (DSSC), and the organic solar cell are the most important representatives for the new generation solar cell (the third generation solar cell). The goal of this generation is breaking the theoretical efficiency limit (Shockley-Queisser Limit [25]) of the solar cell.

One promising device among NSC is the Quantum-Dot solar cell, which is built up of a semiconductor (silicon) coated with a very thin layer of quantum dots. Quantum dots referred to the crystals with diameters in size range of few nanometers. Although the Quantum dots solar cell is still at a pre-commercialization stage, the unique properties (multiple exciton generation effect [27], tunable band gap, large surface area) as well as the potential efficiency of 65% [28] already drawn a large number of photovoltaic researches.

The DSSC was first proposed by B. O'Regan and M. Grazel at UC Berkeley in 1988 [29] and fabricated at EPFL in 1991 [30]. The devices are based on large band gap porous semiconductors attached with dye molecules monolayer. The DSSC has lots of

merits: the simple roll-printing techniques, the low cost raw materials, and the excellent stability. The latest efficiency record for the DSSC is 10.2%. [31]
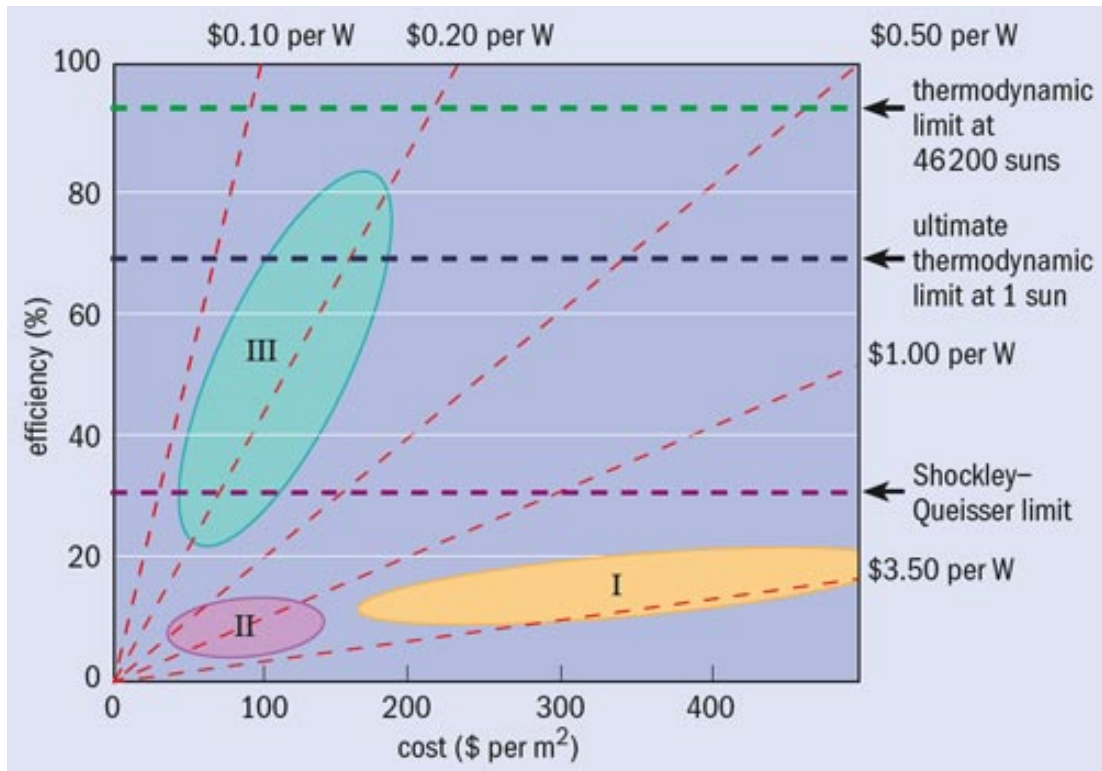
Figure 1.6 The efficiency and cost comparison among

the three generation (I, II, III) solar cells [26]

The research of organic solar cell starts from 1958 by D. Kearns and M. Calvin. [32] The single layer device made by them has a very small efficiency and a large resistance. Due to the poor performance compared with their inorganic counterparts, few researches continued. There is no significant development for organic solar cells

until 1986, when C. W. Tang at Kodak demonstrated a two-layer device (bilayer device). [33] The proposed two-layer device, which is similar with the p/n junction of inorganic solar cell, had an efficiency of 1%.

The invention of Bulk Heterojunction (BHJ) Organic Solar Cells in 1995 by A. Heeger et al. represented a major milestone and a significant improvement in efficiency. [34] The interpenetrating structure of bulk heterojunction largely increases the interface area of acceptor and donor materials. The low manufacture cost, flexibility, as well as the potential high efficiency made the organic photovoltaic research a rapidly progressing field again. Currently, the highest efficiency record for organic solar cells (12%) is held by Heliatek. [35]

To challenge the Shockley-Queisser Limit, several new device configurations have been designed, such as the tandem cell. Tandem cell is the solar cell consisted of several p-n junctions. Each junction of the cell is tuned to absorb light of different wavelength range. The device structure of tandem cell is shown in **Figure** 1.7.
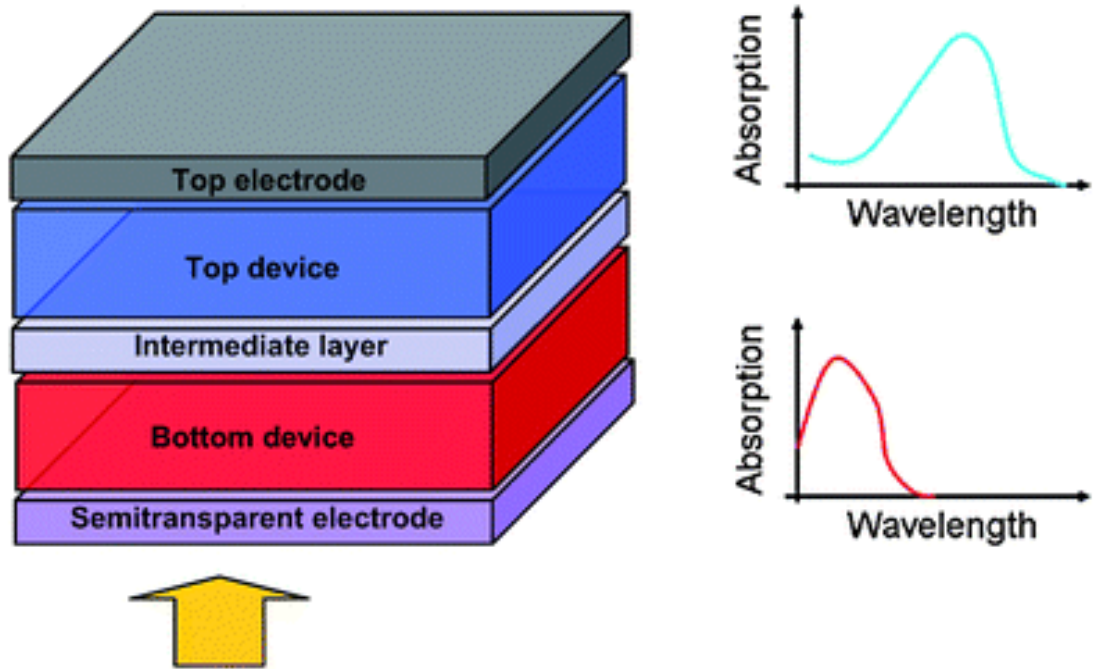
Figure 1.7 Device configuration of the tandem cell and the absorption spectrum of top

device and bottom device [36]

A broad range of policies were implemented to promote the development and

deployment of solar energy in last decade. Without the subsidies from the government

in Germany and Japan, the solar technologies are not fully competitive. There is still a

long way from a lab demonstrator to a commercially cost-effective device for the solar

cell. **Figure** 1.8 displays the latest research developments as well as efficiency records

of each type of solar cells.
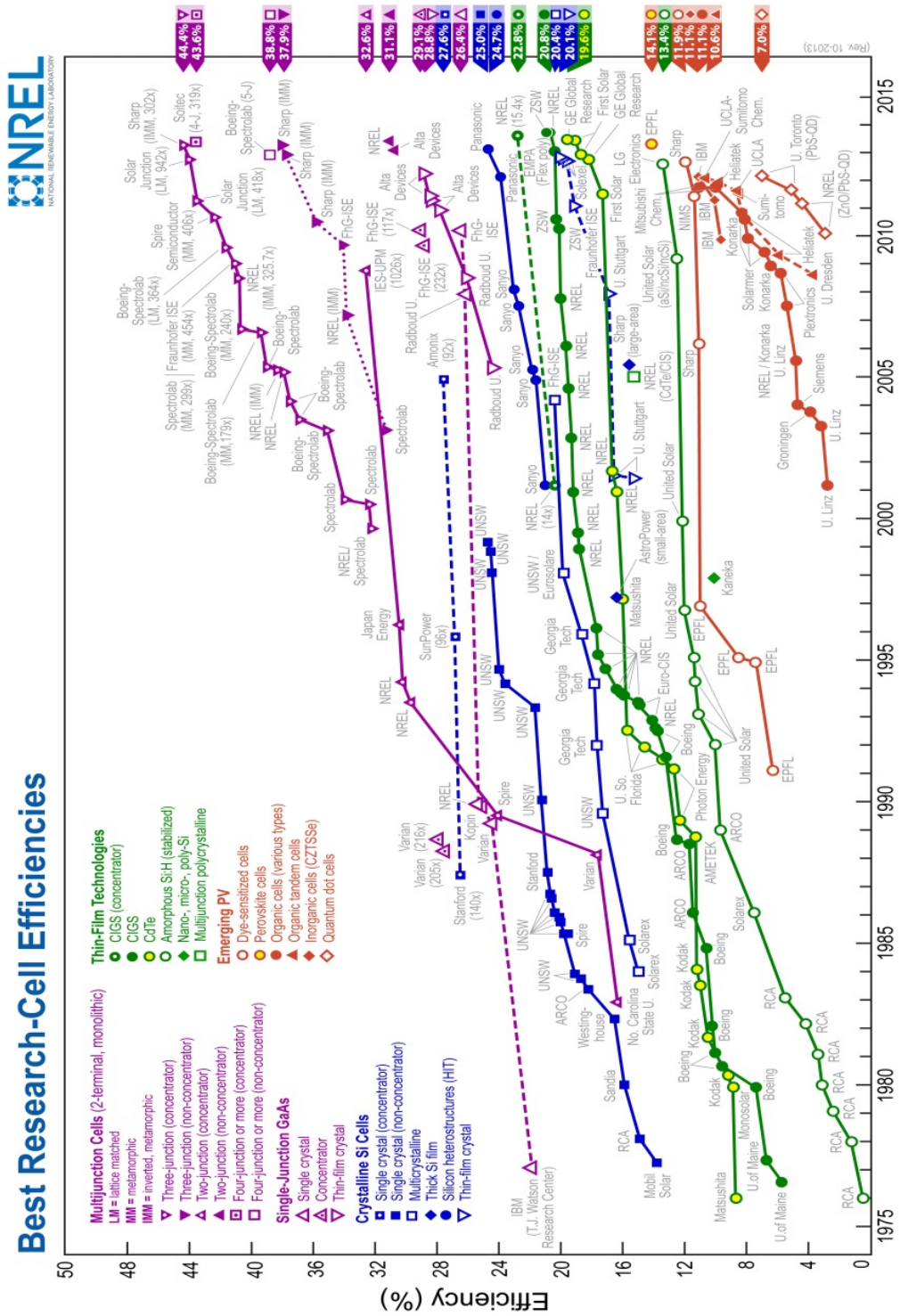
Figure 1.8 Best research-cell efficiencies recorded by the NREL (National Renewable

Energy Laboratory) [37]

1.3 Organic semiconductors

Organic semiconductors (**Figure** 1.9) are the carbon-based materials with backbones comprised of alternating C-C or C=C bonds. The electron configuration for a carbon atom is $1s^2 2s^2 2p^2$. The s and p orbitals could form three sp^2 orbitals while the fourth p_z orbital is left behind. The overlap of p_z electron wavefunctions results in the delocalization of charges, which is responsible for the semiconducting properties of organic semiconductors.
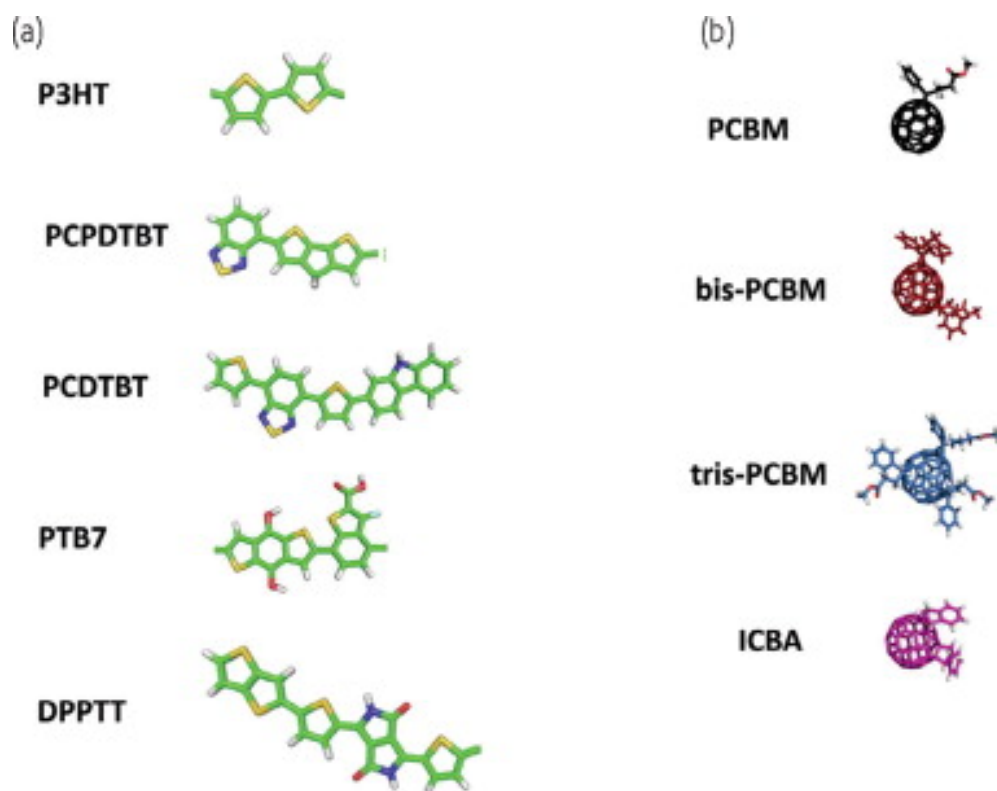
Figure 1.9 Several organic semiconductors for organic solar cells: (a) p-type donor materials; (b) n-type acceptor materials (fullerene derivatives) [38]

The optical and electronic properties of organic semiconductor are vital to the performance of organic solar cell. A comparison between inorganic and organic semiconductors is made.

The first comparison comes from their absorption ability on sun light. Organic semiconductors usually exhibit very high absorption coefficients (about 10^7 m^{-1}) and a thin film with a thickness of 100 – 300 nm is sufficient for a good absorption yield for photovoltaic application. However, an absorber layer of several micrometers is required for the second generation solar cell and more than 100 micrometers for single crystalline silicon solar cell.

Despite the advantage, the organic semiconductors could only absorb a finite range of solar spectrum due to the narrow absorption width (large energy gap). The energy gap of a conjugated polymer is about 2 eV (absorption range: visible spectrum), while for inorganic semiconductor silicon the band gap is just 1.1 eV (absorption range: the whole visible spectrum, and beyond to 1000 nm). Several methods of molecular modification were adopted to reduce the energy gap of organic semiconductors, such as the introduction of bridging atoms [39].

The largest difference between inorganic and organic semiconductor is the fact that the excited states in organic semiconductor are localized. The generated exciton, created from the absorption of a photon, is localized on a single molecule or a single

15

conjugated segment within a volume of few cubic nanometers in organic semiconductors. However, the dielectric constant of organic semiconductor is very low ($\varepsilon \approx$ 3~4) compared with their inorganic counterpart (for silicon, ε = 11.8). This directly results in their distinct exciton dissociation processes. We can assume the generated exciton as a Coulomb-bonded electron-charge pair with a separated distance of 1 nanometer. The calculated binding energy for organic semiconductor is about 0.5 eV, which is much larger than the thermal energy at room temperature (E_{th} = 0.02585 eV). This kind of tightly bound exciton is defined as "Frenkel Exciton" while the weakly bound exciton in inorganic semiconductors is termed as "Wannier-Mott Exciton". Since the generated exciton could be easily dissociated as their inorganic counterpart, external forces such as electric field are needed for the charge separation.

Most of the organics, especially the conjugated polymers, are not crystalline materials. The disordered structure makes the charge carrier transport mainly in a hopping mechanism, which is less effective than the band transport in inorganics.

In spite of those shortcomings, the low cost, ease of manufacture by printing or spin-coating from solution made it possible for the large scale commercialization. A brief comparison is summarized in **Table** 1.1.

Table 1.1 A comparison between organic and inorganic semiconductors

	Inorganic Semiconductors (Silicon)	Organic Semiconductors (P3HT)
Absorption Thickness	~100 um	~100 nm
Energy Gap Width	1.1 eV	1.9 eV
Dielectric Constant	11.8	Usually 3~4
Exciton Type	Wannier-Mott Exciton	Frenkel Exciton
Charge Transport Method	Band transport	Hopping mechanism

1.4 Metal-semiconductor and Metal-insulator-Metal structures

1.4.1 Metal-semiconductor contacts
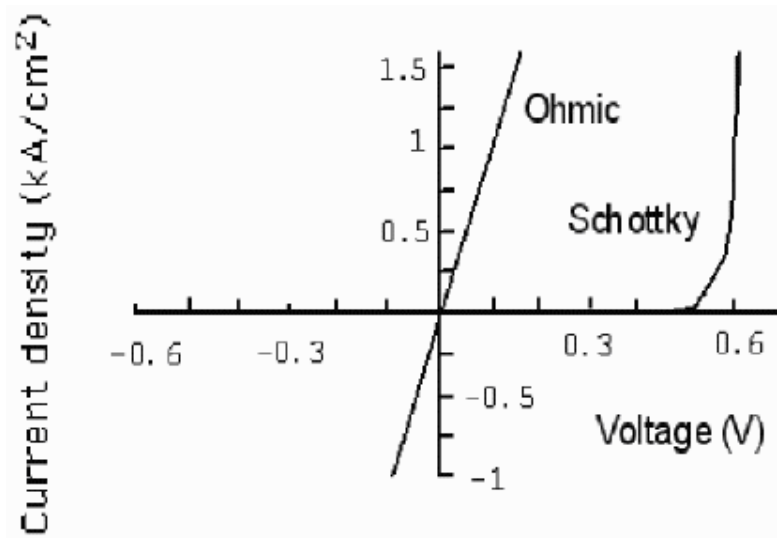
Figure 1.10 The current density-voltage characteristics of Schottky and Ohmic

Junction

There are two different types of metal-semiconductor contacts: the Schottky Junction and the Ohmic junction. Their current density-voltage characteristics of them are plotted in **Figure** 1.10.

The rectifying current-voltage characteristics of Schottky Junction are very similar to those of the p/n junctions, except for several differences. One of them is that the Schottky Junction only has a single type of charge carrier. The energy diagram of p-type Schottky Junctions is exhibited in **Figure** 1.11.
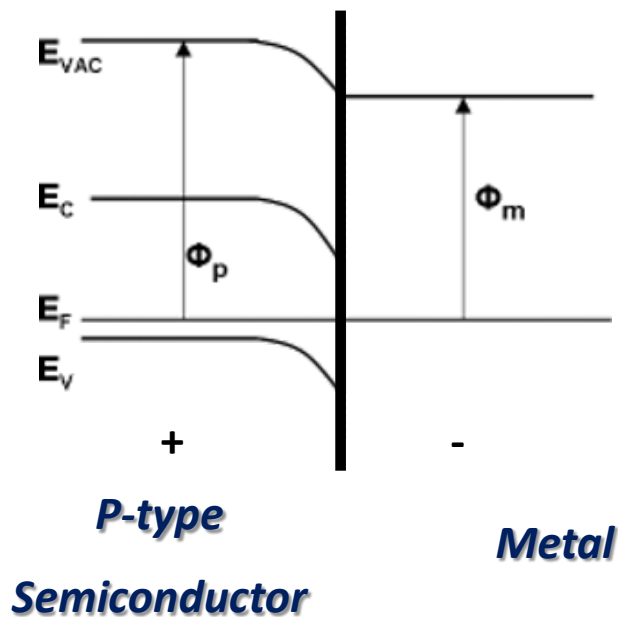
Figure 1.11 The energy diagram of p-type Schottky Junctions

As a low resistance junction, the Ohmic Junction provides current conduction from metal to semiconductor and vice versa. The electric characteristic of the contact

is equivalent to that of a small resistance. A typical Ohmic junction between metal and

p-type semiconductor is shown in **Figure** 1.12.

P-type

Semiconductor

Metal

E_{VAC}

Φ_p

Φ_m

E_C

E_F

E_V

-                    +
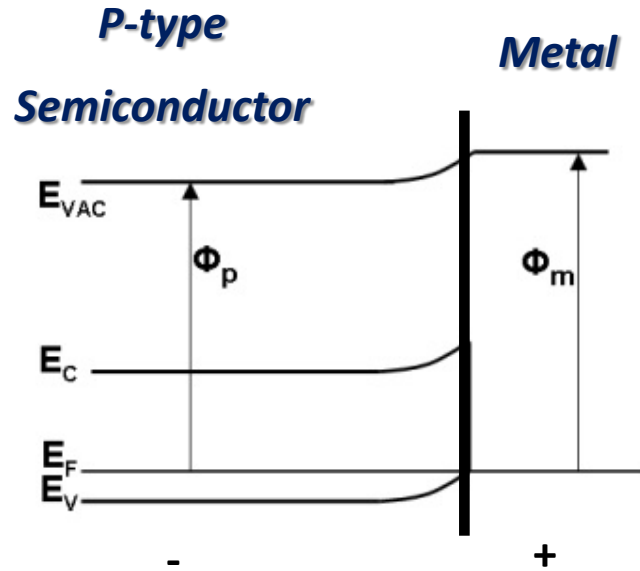
Figure 1.12 The energy diagram of Ohmic Junctions

1.4.2 Metal-insulator-Metal structures

Metal-insulator-Metal (M-i-M) structures, is the rectifying structures comprised of

insulators and metals. Two metals with asymmetrical work functions are put together

with an insulator sandwiched between. The energy diagram of the structure is

determined by the work functions of the metals, the conduction band and band gap of

the insulator. In most case, the band gap of the insulator is so large that the valence

band of it exists outside of the presented energy diagram scale in **Figure** 1.13. The tilt

line of the band is due to the internal electric field caused by the work function

difference between the two electrodes.
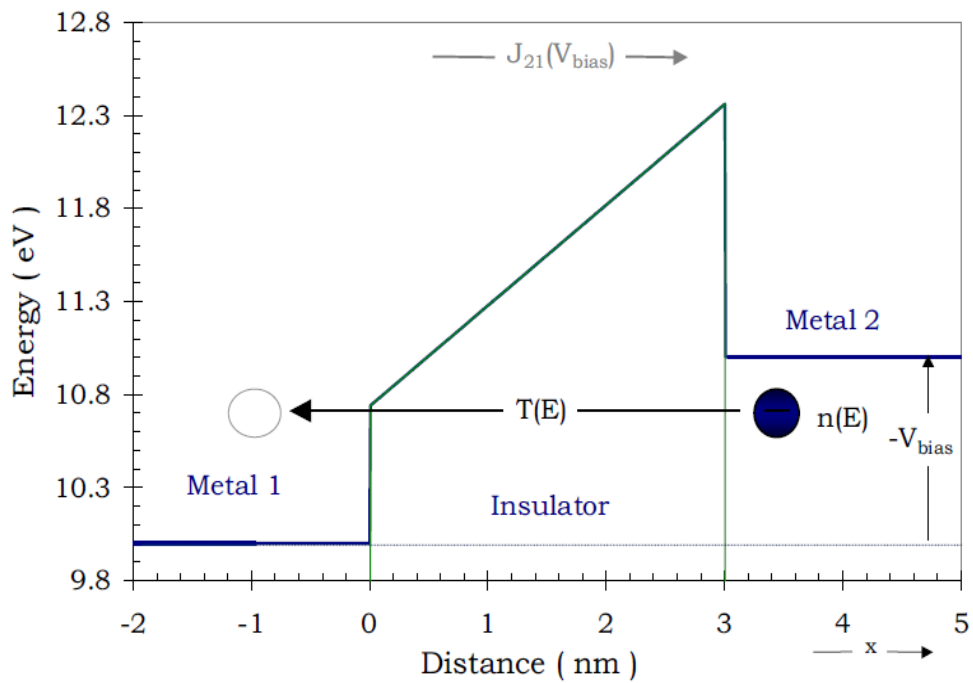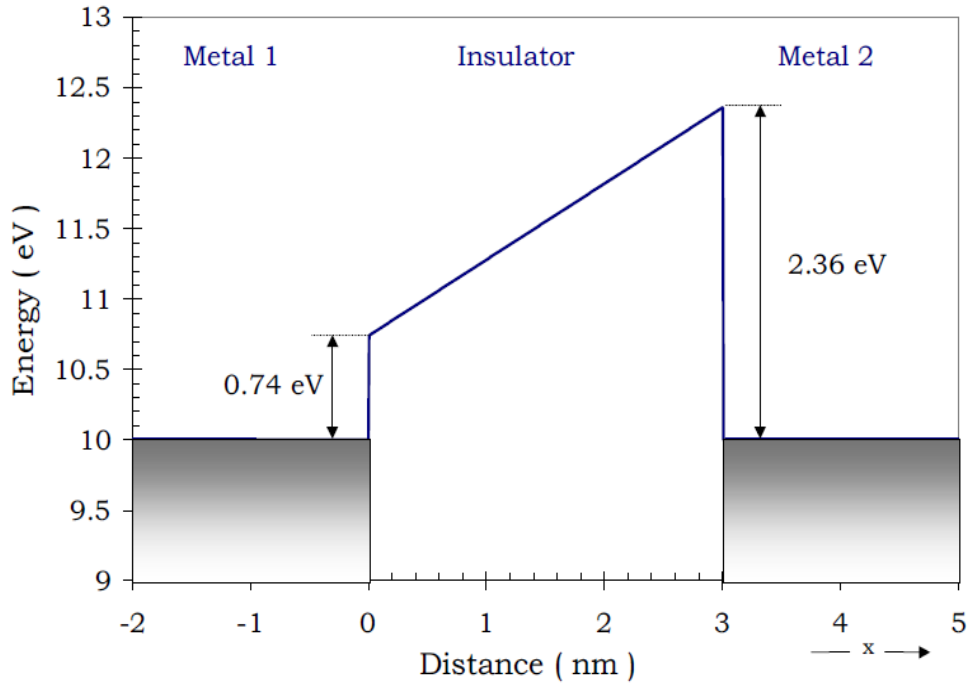
Figure 1.13 The energy diagram of M-i-M structure [40]

Tunneling is the predominant charge carrier transport mechanism in M-i-M structures. Under applied bias voltage, the tunneling of electron through the forbidden insulator region could be possible, especially when the thickness of the layer is rather small (<10 nm). This model is widely used in the explanation of the operation mechanism of organic electronic devices, especially in OLED and OPV researches.

1.5 Current challenges for organic photovoltaics

Over the last 30 years, significant interest in utilization of organic photovoltaics has produced rapid improvement in device efficiency and stability. However, many of the processes that lead to the low efficiency still remain poorly understood, posing an enormous challenge for the future efficiency enhancement.

Shockley-Queisser Limit (**Figure** 1.14) [25], or detailed balance limit, is the mostly used theoretical model for maximum efficiency calculation for a p-n junction solar cell. According to the curve, the largest efficiency the organic photovoltaic could reach is about 23%, which is much higher than the current record (~10%). [41]
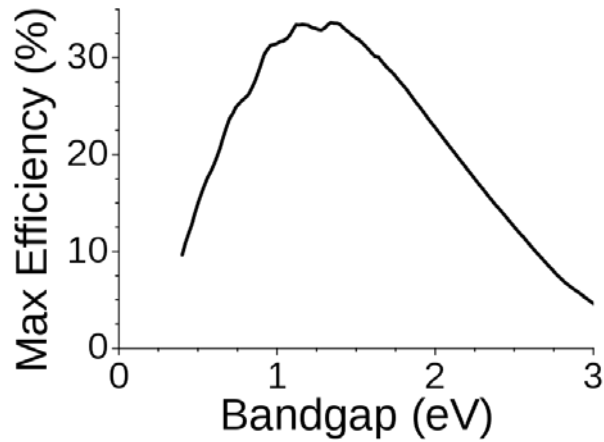
Figure 1.14 The Shockley-Queisser Limit for the efficiency of a solar cell

Some possible factors that may result in the efficiency loss include spectrum loss, exciton loss, recombination loss, and contact loss.

Many methods are proposed including the synthesis of new chemicals, and the novel device structures. However, the poor understanding of the device physics made most of the efforts become trial-and-error jobs. The problems on several important processes such as charge separation, and charge transport still remain controversial. Many further researches are needed to find the most optimized procedures for high efficiency devices and the promising way for large scale production.

1.6 Thesis overview

The thesis contains five chapters. *Chapter 1* made a brief introduction on the major

concepts involved in this study, including the history of solar cells, the basics of organic semiconductors, the development of organic solar cells, as well as the commonly used energy diagrams for bulk heterojunction solar cells, which are key tools for analyzing the device physics. It is followed by the detailed literature reviews in *Chapter 2*. An overview was given on the working principle and operating parameters of organic solar cells. However, the controversies of energy diagram of bulk heterojunction solar cell remain unsolved.

Chapter 3, Experimental Procedures, includes the details of device fabrication, power conversion efficiency measurements for our study. Results and finding of the experiments are discussed in *Chapter 4*. Finally, the main conclusions of this study are summarized in *Chapter 5*.

Chapter 2 Literature Review

2.1 Operation mechanism of photovoltaics

The discovery of new semiconductors and the introduction of p/n junction result in the large development of device physics of photovoltaics. Currently, the generally accepted working principle of a solar cell is concluded in three steps: (i) exciton generation and diffusion; (ii) charge carrier pair separation; (iii) charge carrier transport and extraction. And we will describe the details of those processes in this section. .

2.1.1 P/N junction and internal electric field

The basic electronic properties of a semiconductor could be explained in a simplified two-dimensional crystal models (**Figure** 2.1). The hole is the majority carrier in p-type doping region, and the n-type doping region has a large concentration of electrons. When the two regions are connected, holes would diffuse from the p part to the n part because of the concentration gradients; whereas the converse is true for the

electrons in n part.
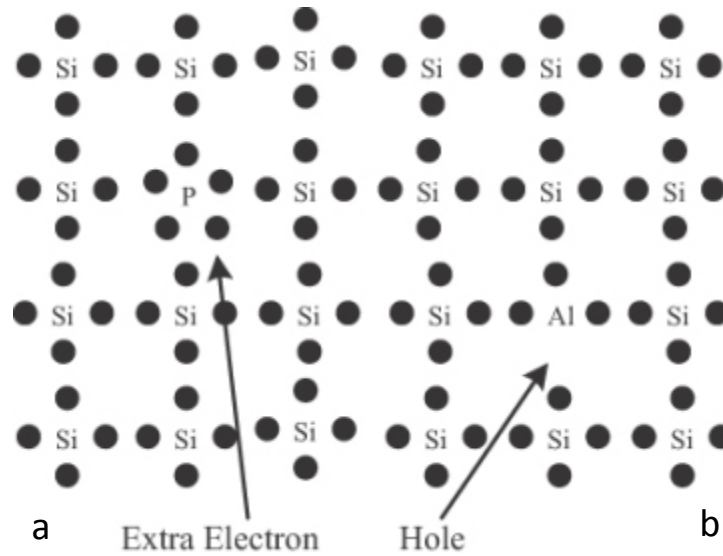
Figure 2.1 Two-dimensional representations of n-type doping (a) and p-type doping (b)

silicon crystal

The diffusion of carriers could be considered as a recombination process of the

electrons and holes, which leads to the formation of depletion layer. There are fewer

majority carriers in the depletion layer than there in the electroneutral region, which

results in an uncompensated charge of fixed acceptor (negative) and donor ions

(positive). The space charge creates the internal electric field as shown in **Figure** 2.2.

The drift current caused by the internal electric field is in the opposite direction of the

diffusion current. When equilibrium state is attained, the net current through the

circuit is equal to zero.

The built-in voltage caused by the electric field is given by:

$$V_{bi} = V_t In \frac{N_D N_A}{N_i^2}$$

where N_D and N_A are the space charge density of the donor and acceptor, and N_i the carrier density of intrinsic semiconductor, V_t the thermal voltage.
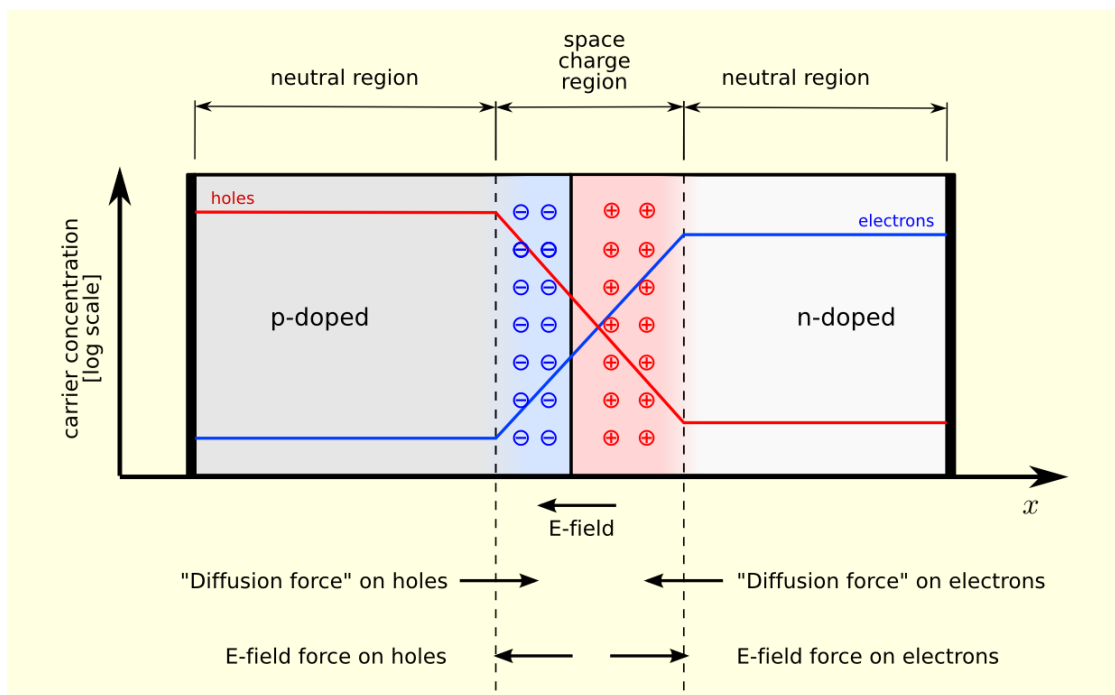
Figure 2.2 The formation of internal electric field in p/n junction [42]

2.1.2 Exciton generation and diffusion

The incident photons will be absorbed by the semiconductor materials, reflected by the surface, or transmitted through the materials. The reflection and transmission are considered as important efficiency loss mechanism in photocurrent conversion. The

main parameter determining the absorption of a photon is the energy of the photon. The photon could be absorbed only when the energy of the photon is enough to excite the electron from the valence band to the conduction band. The maximum wavelength of the light that can generate exciton could be calculated by

$$\lambda_{max} = \frac{hc}{E_g}$$

where h is the Planck Constant, c the speed of light, and E_g the band gap of the semiconductor.

An electron-hole pair (exciton) is generated after the absorption of photon. Through the diffusion, the created excitons could be transported to the internal electric field for separation. However, some of them could recombine when they could not be separated within their lifetime. The recombination would release the energy by giving off a photon or phonon.

2.1.3 Charge carrier pair separation

The band bending due to the internal electric field is good enough for the created electrons and holes to easily roll down or bubble up within the depletion layer. The value of photocurrent is determined by the ratio of exciton pair generated by the light, which could be increased by the illumination intensity.
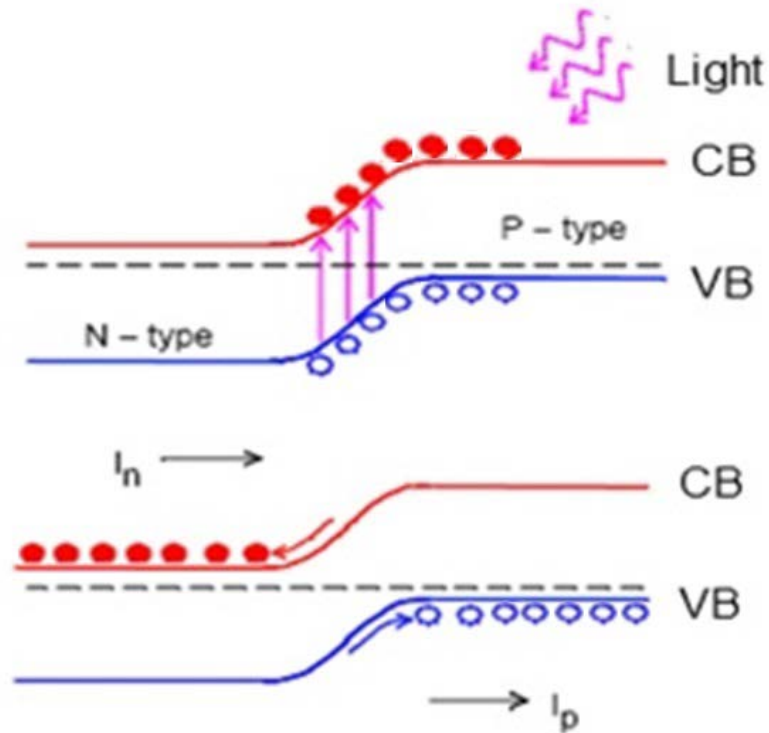
Figure 2.3 The photon generation and charge carrier pair separation [43]

The dielectric properties (ε) of semiconductor discussed in the Section 1.3 is crucial to the charge carrier pair separation process. The energy required to separate the pairs could be estimated by

$$E_{Separation} = \frac{e^2}{4\pi\varepsilon r}$$

where the e is the elementary charge, r the distance between the two charge carriers.

In inorganic solar cells, the excitons could be easily separated by the thermal energy (0.02585 eV) provided by the room temperature. However, the driving force for

the exciton dissociation in organic solar cells (especially the Bulk Heterojunction Solar Cells) remains controversial. [38]

2.1.4 Charge carrier transport and extraction

After the charge pair separation, the charge carriers would be transported to the corresponding electrodes and produces the output current. In addition to the drift current due to the built-in electric field, the diffusion current mechanism is caused by the concentration gradient of the charge carriers.

Drift current is determined by the conductivity σ of the materials and the electric field density E:

$$j_{drift} = \sigma E.$$

The σ of a semiconductor is given by:

$$\sigma = qn\mu_n + qp\mu_p$$

where q is the elementary charge, n and p the concentration of electrons and holes, and μ_n and μ_p the mobilities of electrons and holes respectively.

Diffusion current is characterized by the Fick's fist law:

$$j_{diffusion} = qD\frac{d\rho}{dx}$$

where D is the diffusion coefficient of the charge carriers (holes or electrons), and $d\rho/dx$ represents the flux density. [44]

In inorganic solar, the band transport is the dominant mechanism while for

disordered materials as conjugated polymers, charge carriers mostly use hopping method for transport. In the organic semiconductors, the localized charge carriers hops between two neighboring sites when the wave functions of the given orbital do not overlap strongly. [45] The hopping mechanism leads to the small mobility and poor charge transport of the organic semiconductors.

During the transport process, the charge carriers could also recombine. Geminate recombination refers to those carriers share the same precursor state in contrast to the non-geminate (bi-molecular) recombination. Geminate recombination is a unique phenomenon observed in the organic photovoltaics due to the difficult charge separation processes (Frenkel Exciton). In addition, the low mobility of organic semiconductors as well as the possible interrupted transport path caused by interpenetrating morphology largely increases the probability of the non-geminate recombination. However, the recombination rate could be largely reduced by a fine control of the internal microstructure of the bend. [46]

In the end, the dissociated charge carriers that do not recombine are collected by the corresponding electrodes and yield an output current.

2.2 Device development of organic photovoltaics

2.2.1 Single layer devices

The emergence of the organic photovoltaics is usually attributed to the discovery of semiconduction in organic molecular substances. The organic photovoltaic device was first witnessed by D. Kearns and M. Calvin in 1958 when they made a laminated device by employing magnesium phthalocyanine (MgPh) and air-oxidized tetramethyl p-phenylenediamine (TMΦD). [32] Although their output voltage could arrive 200 mV, the maximum power produced was only $3*10^{-12}$ W.

Some following researches started to replace chemicals for the organic layer and sandwiched it in between two dissimilar metal electrodes, typically a layer of indium tin oxide (ITO) and a high work function metal layer (Aluminum, Calcium, or Silver). [47] It is the simplest device configuration for the various types of organic photovoltaics. A sketch of the single layer devices is displayed in **Figure** 2.4.
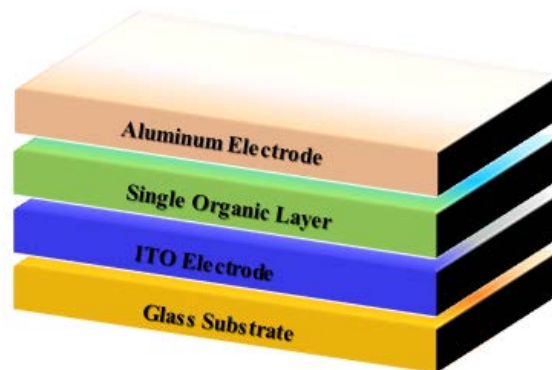
Figure 2.4 Single layer OPV devices (structure: Al/Organic/ITO)

As illustrated in the M-i-M structure, the single organic layer could be

considered as an ultra-thin insulator film. The work function difference between two metals provides an internal electric field across the organic layer. The exciton generated in the organic layer will be separated by the built-in electric field. Holes were transported to the ITO electrodes while electrons were pulled towards the aluminum side. The produced current could be used to work. This model is called the M-i-M model in the literature. [48] The energy diagram of such a device is shown in **Figure** 2.5. The photovoltaic properties of the single layer device strongly rely on the choice of the electrodes.
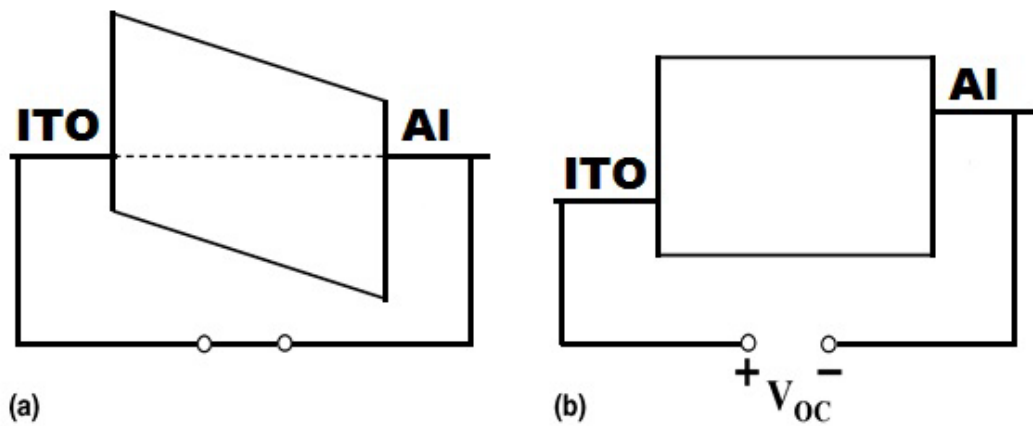
Figure 2.5 The energy diagram of single layer devices in M-i-M model:

(a) short-circuit condition and (b) open-circuit condition

However, it is not always correct to consider the organic layer as an insulator.[49] The polymer would easily be p-doped placing in oxygen and moisture

environment. In the following revised model, the insulator was replaced by a p-type semiconductor. [50] And a Schottky Junction would be formed between the aluminum electrode and the organic. The energy diagram of the revised model is schemed in **Figure** 2.6.
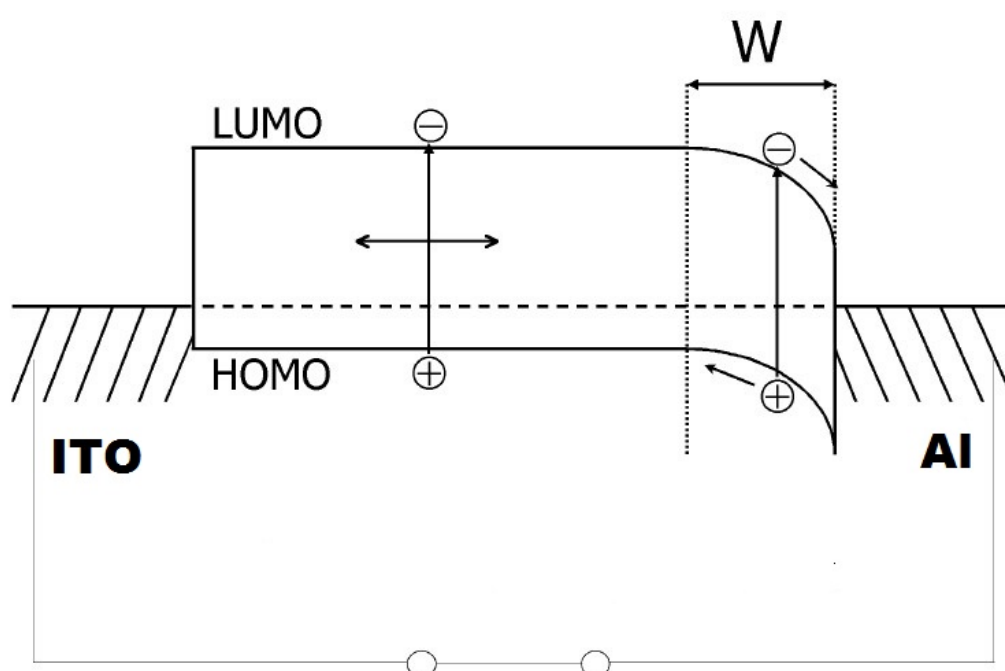
Figure 2.6 The energy diagram of single layer devices in p-type Schottky Junction

model

The bending region (W) close to the Schottky Junction corresponds to an electric field in which the exciton could be broken up. Due to the finite exciton diffusion length (<20 nm) in organic semiconductors [51], only the excitons generated

in the vicinity of the junction could contribute to the photocurrent.

The low efficiency (less than 1%), resulted from the poor charge transport and insufficient charge separation, limits the further development of the single layer device.

2.2.2 Bilayer heterojunction devices

It is easy to build an internal electric field in an inorganic semiconductor through the accurate control of p-type or n-type doing. However, most of the polymers used in the OPV are pure or intrinsic semiconductors due to the difficulty of doping control. In order to generate a built-in electric field, incorporating another semiconductor to form a p/n junction structure could be a practical way. The electron acceptor/donor structure is termed as the bilayer heterojunction device of OPV.

The first two-layer OPV device (bilayer Heterojunction device) was demonstrated by C. W. Tang at Eastman Kodak Company in 1986. [33] Two different organic semiconductors were applied: copper phthalocyanine (CuPc) as the electron acceptor and perylene tetracarboxylic derivative (PV) as the electron donor. The device configuration as well as the current-voltage characteristics of the device is shown in **Figure** 2.7.
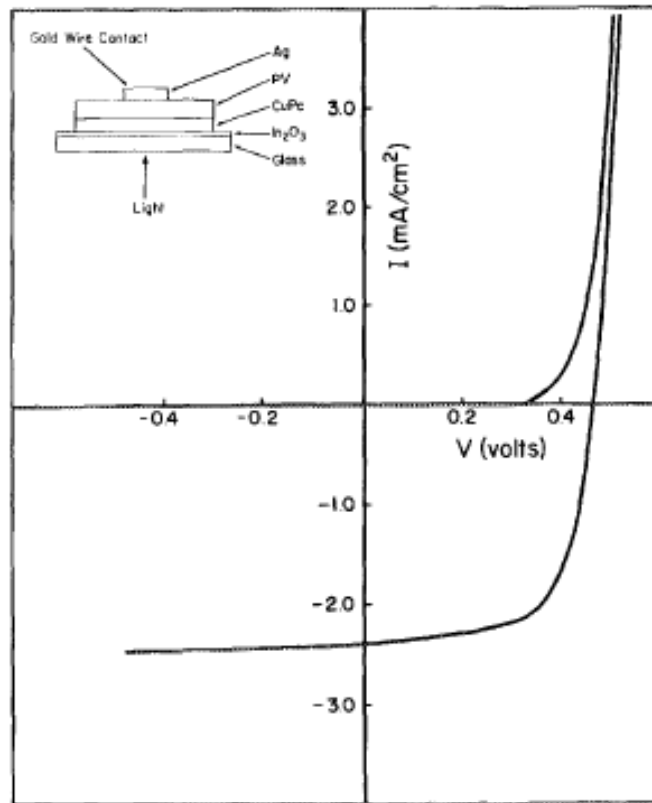
Figure 2.7 The device configuration and I-V curve of the first bilayer OPV device

The device achieved the efficiency of about 1% and a fill factor of 0.65, which is much higher than most of the single layer device. Tang revealed that the interface between two thin organic layers is the crucial determinant for the output voltage. The generated exciton within several nanometers of the heterojunction will diffuse to the interface and be segregated as depicted in **Figure** 2.8.
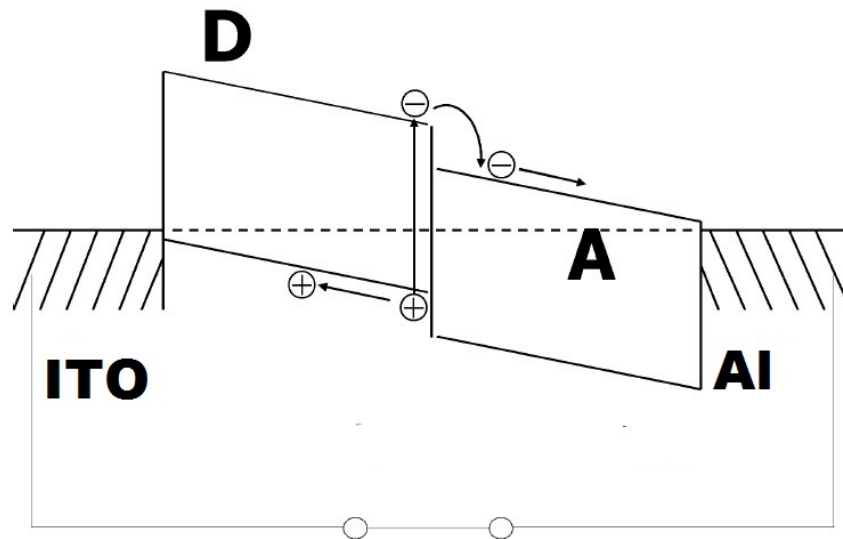
Figure 2.8 The energy diagram of the bilayer heterojunction devices

The monomolecular charge transport is the biggest advantage of the bilayer device, in comparison with the single layer device. In the bilayer device, the electrons are transported in the acceptor domains, while the holes travel within the donor regions. This mechanism effectively separates the two charge carriers by different transport routes and largely reduces the possibility of geminate recombination. [45] The performance optimization of bilayer device is a trade-off between the absorption thickness and diffusion length. Hence, there is still much room for the efficiency promotion. [52]

2.2.3 Bulk heterojunction devices

The concept of bulk heterojunction (BHJ) was first proposed in 1995 by Alan Heeger et al. [34] In a BHJ device, the electron donor and acceptor are blended intimately in a bulk volume so that the distance between the donor-acceptor interface and the exciton generation sites is always within the exciton diffusion length. The bulk heterojunction layer could be processed by co-evaporation or solution casting of the blend. Similar with the single layer device, two different energy diagrams were used by the community: The M-i-M model (Figure 2.9) [53] and the P-type Schottky Junction Model (Figure 2.10) [54].
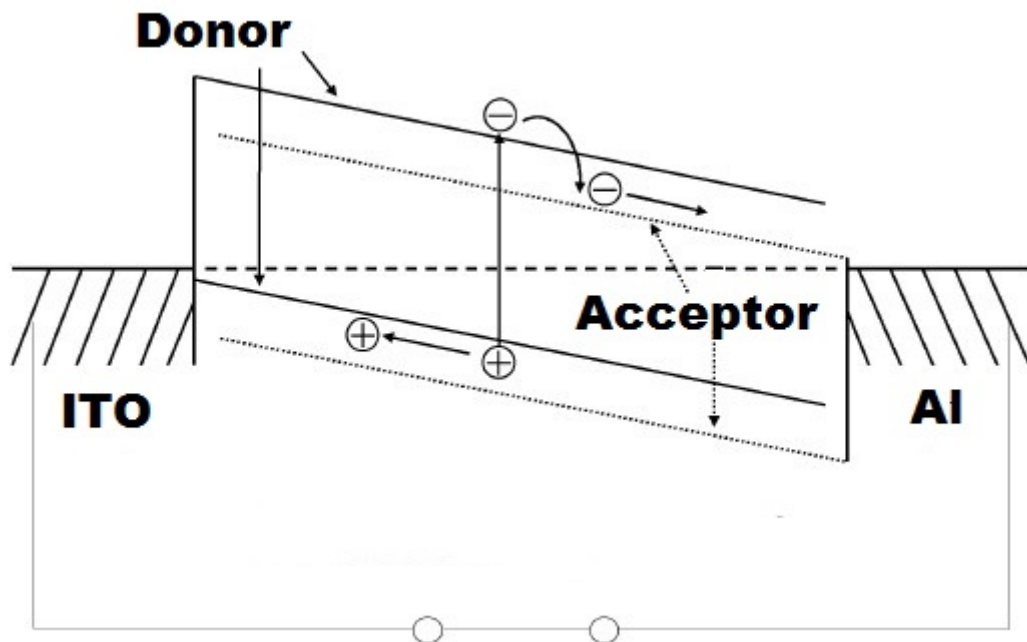
Figure 2.9 The energy diagram of the bulk heterojunction in M-i-M model
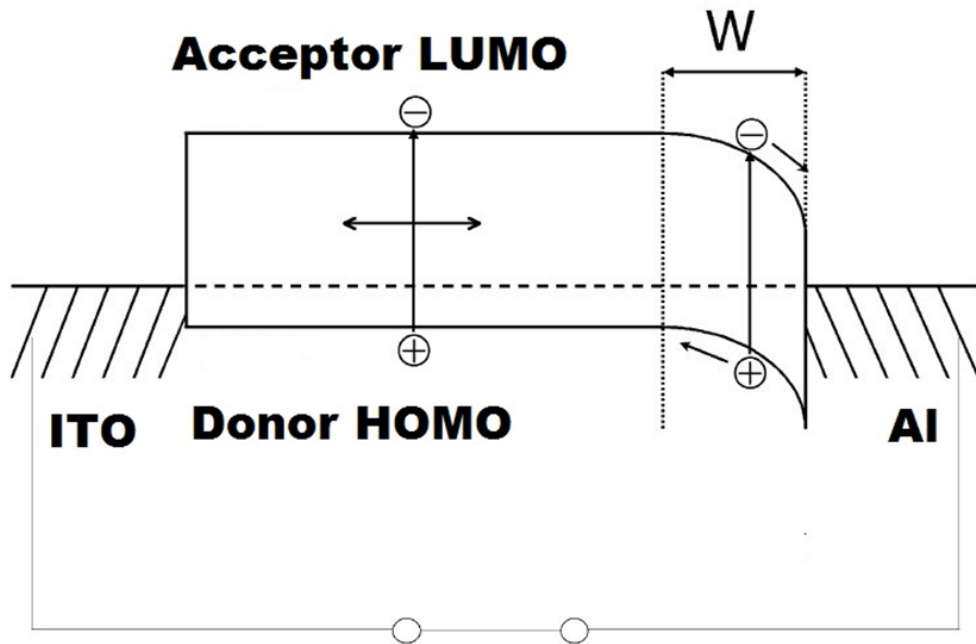
Figure 2.10 The energy diagram of the bulk heterojunction in p-type Schottky

Junction model

A spatial bicontinuous morphology is mandatory for a better performance of the bulk heterojunction device. Many kinds of treatment had been used for a better control of the morphology of the bulk heterojunction, such as the thermal annealing[55], and solvent-vapor treatment[56]. As reported by Ma et al., through the post-production annealing at 150° C, the P3HT/PCBM bulk heterojunction solar cell could have an efficiency of 5%, which is the highest record for the system. [46] The solvent-vapor treatment proposed by Yang et al. had a similar enhancement: the solvent molecules made a contribution in the phase reorganization, and crystallization to improve the

morphology. [57]

2.2.4 Diffuse bilayer heterojunction devices

The diffuse bilayer heterojunction is proposed based on the design of the bulk heterojunction, and its scheme is shown in **Figure** 2.11. This type of devices successfully avoids the interrupted pathway for the charge transport, which is the largest shortcoming of bulk heterojunction. The diffuse interface could be processed in several ways, such as the annealing control of a bilayer device [58].
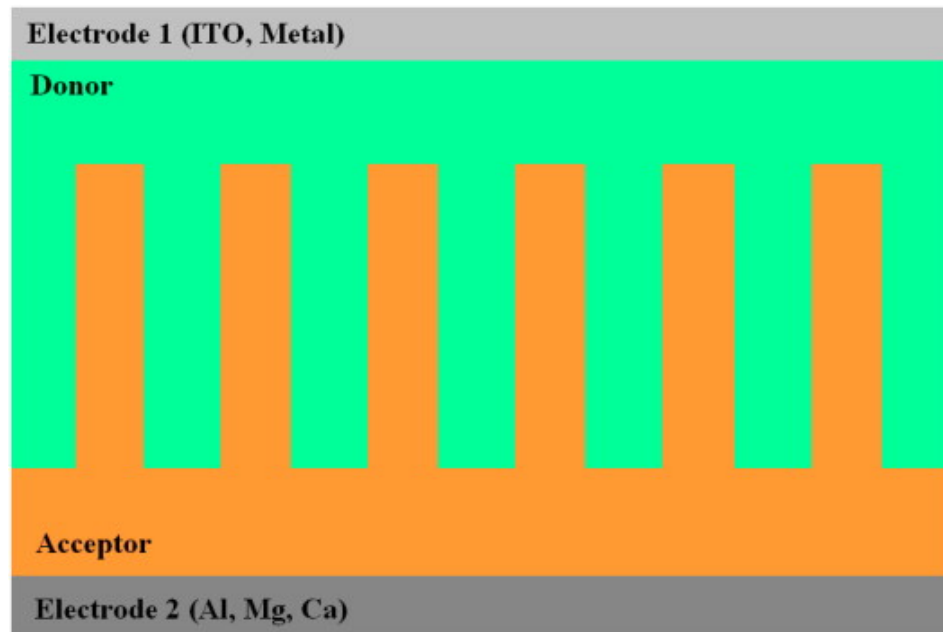
Figure 2.11 Diffuse bilayer heterojunction devices [59]

2.3 Measurements of power converting efficiency

Power Converting Efficiency (η) is the most significant feature to evaluate the performance of a solar cell. The η value is based on four parameters: incident radiant power $P_{incident}$, open circuit voltage V_{oc}, short circuit current density J_{sc}, and fill factor FF. And the η is given by

$$\eta = \frac{V_{oc}J_{sc}FF}{P_{incident}}.$$
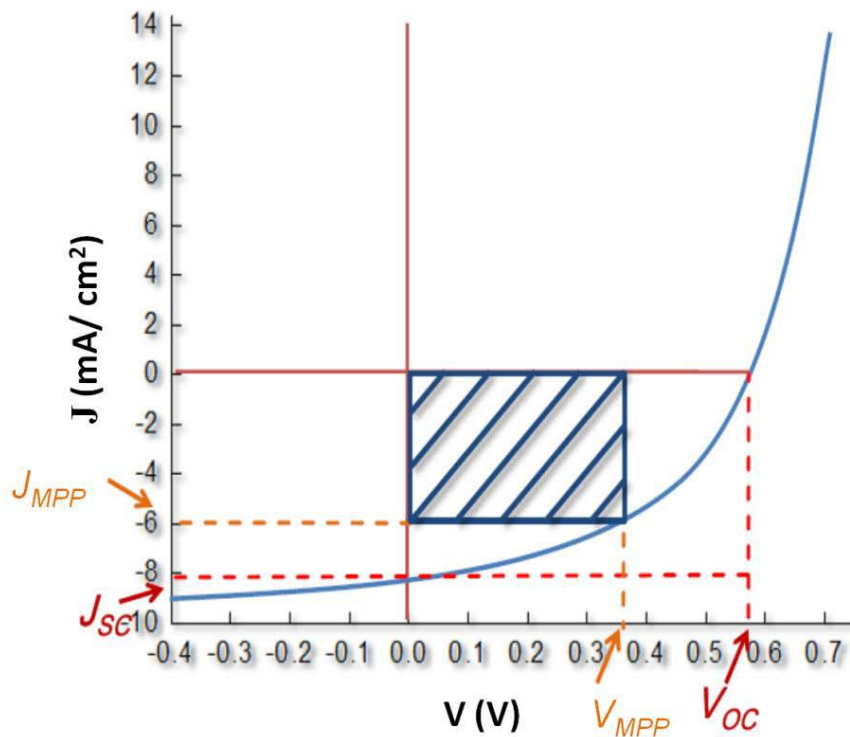
Figure 2.12 A typical Current Density-Voltage Characteristics of a solar cell [60]

The V_{oc} is defined as the maximum voltage a device could produce when the nodes are isolated. The maximum current a device could be measured when the nodes are connected is termed as J_{sc}. FF is the ratio of maximum power (the product of V_{MPP} and J_{MMP} in Figure 2.12) to the product of the open circuit-voltage and the short-circuit current. Generally, the value of FF represents the "squareness" of the current density -voltage characteristics. All the information could be measured from the current density-voltage curve of the device (**Figure** 2.12).

The generated photocurrent (Jsc) under illumination could be calculated through the integral formula:

$$J_{sc} = qA^{-1} \int \emptyset(\lambda) EQE(\lambda) d\lambda \quad \text{(Eq. 2.2)},$$

where q is the elementary charge, A the effective area for exciton absorption, $\emptyset(\lambda)$ the incident photon flux at each wavelength λ, and $EQE(\lambda)$ the external quantum efficiency of the device. Quantum efficiency indicates the amount of current that the cell could generate when absorbing photons at each wavelength. For solar cells, two types of quantum efficiency are commonly used: External Quantum Efficiency (EQE) and Internal Quantum Efficiency (IQE).

$$IQE = \frac{N_0 (Charge\ Carriers\ Collected\ By\ Solar\ Cells)}{N_1 (Absorbed\ Photon)}$$

$$EQE = \frac{N_0 (Charge\ Carriers\ Collected\ By\ Solar\ Cells)}{N_2 (Incident\ Photon)}$$

IQE represents the active layer's ability of photon absorption. The EQE is always smaller than the IQE and independent of the incoming light spectrum.

The solar cells share similar rectifying current density- voltage behavior with the diodes. The Shockley diode equation for inorganic devices has already been widely applied in the organic solar cell researches. To describe a real solar cell, several other elements are added, including the current source (j_{sc}), series resistor (R_s), and shunt resistor (R_{sh}). The modified Shockley equation [61] is given as:

$$j(V) = j_0 \left\{ exp \left\{ \frac{q(V - jR_s)}{nkT} \right\} - 1 \right\} - \frac{V - jR_s}{R_{sh}} - j_{sc}$$

where j_o is the saturation current density, q the elementary charge, kT the thermal energy, and n the diode ideality factor. The corresponding equivalent circuit is depicted in **Figure** 2.13.
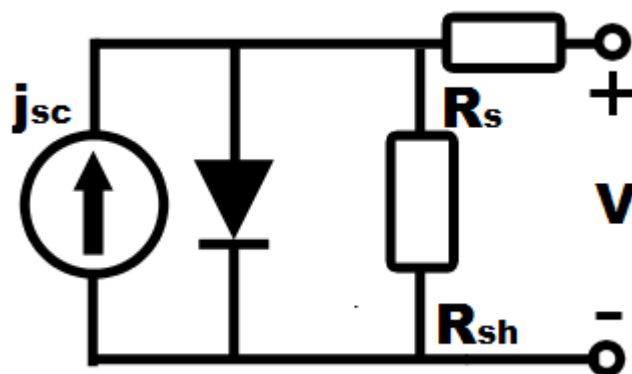
Figure 2.13 The equivalent circuit of a conventional solar cell

R_s usually represents the resistance caused by the contacts, such as the injection barriers and sheet resistances; while the R_{sh} refers to the influence of current leakage between two electrodes, such as the losses due to some additional peripheral current paths. To improve the efficiency of the device, R_s should be reduced and R_{sh} should be increased as shown in **Figure** 2.14.
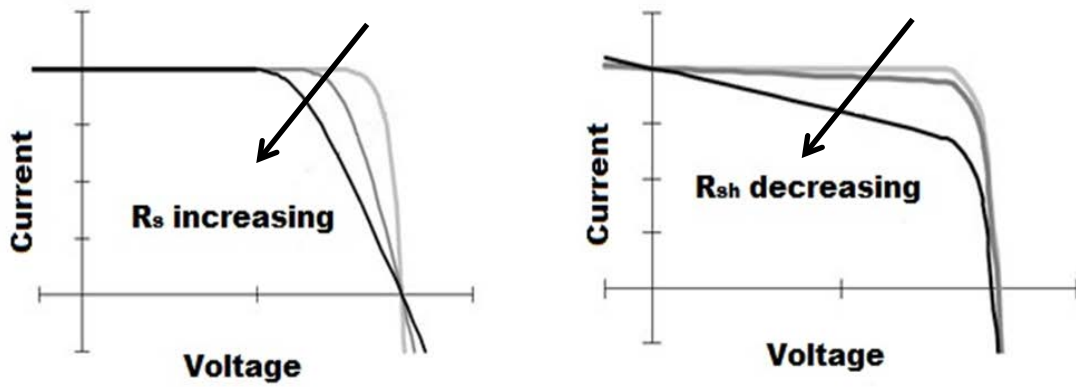
Figure 2.14 Effects of R_s and R_{sh} on the photovoltaic performance [62]

Chapter 3 Experimental Procedures

3.1 Device fabrication

3.1.1 Chemicals for experiment

The electron donor Poly(3-hexylthiophene-2,5-diyl) (P3HT) and the electron acceptor [6,6]-Phenyl C_{61} butyric acid methyl ester (PCBM) were purchased from 1-material Chemscitech and used as received. P3HT and PCBM dissolved separately in 1,2-dichlorobenzene (DCB) solution with a weight ratio of 1:1 for blend use. The Poly(3,4-ethylenedioxythiophene)-poly(styrenesulfonate) (PEDOT:PSS) was obtained from Aldrich. The chemical formulae of them are shown in **Figure** 3.1.

3.1.2 Conventional organic photovoltaic devices

The structure configuration of a conventional device is ITO/ PEDOT:PSS/ P3HT:PCBM/ Al. The device is usually prepared on pre-cleaned ITO/glass substrate. A PEDOT:PSS thin film with a thickness of 40 nm is then spin coated. After a 10-minute drying process at 120 °C, the prepared polymer blend (P3HT and PCBM)

was spin-coated on top of the device. The active layer was allowed to dry in the DCB

ambience for 2 to 3 hours. All of the above processes are conducted in glove box filled

with Nitrogen (N_2). Finally, an Aluminum (Al) cathode was deposited onto the

half-finished device by a vacuum evaporation system.
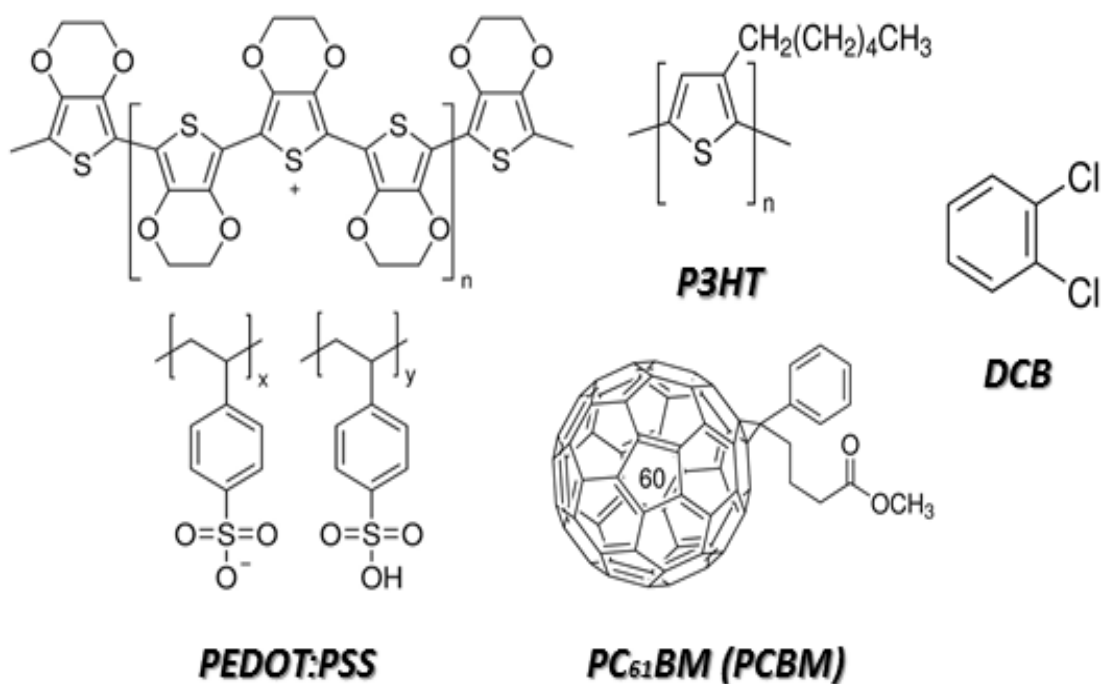
Figure 3.1 Conjugated polymers and organic molecules used in our experiment

3.1.3 Symmetric electrode organic photovoltaic devices

The device configuration of a symmetrical electrode organic photovoltaic device is

exhibited in **Figure** 3.2.
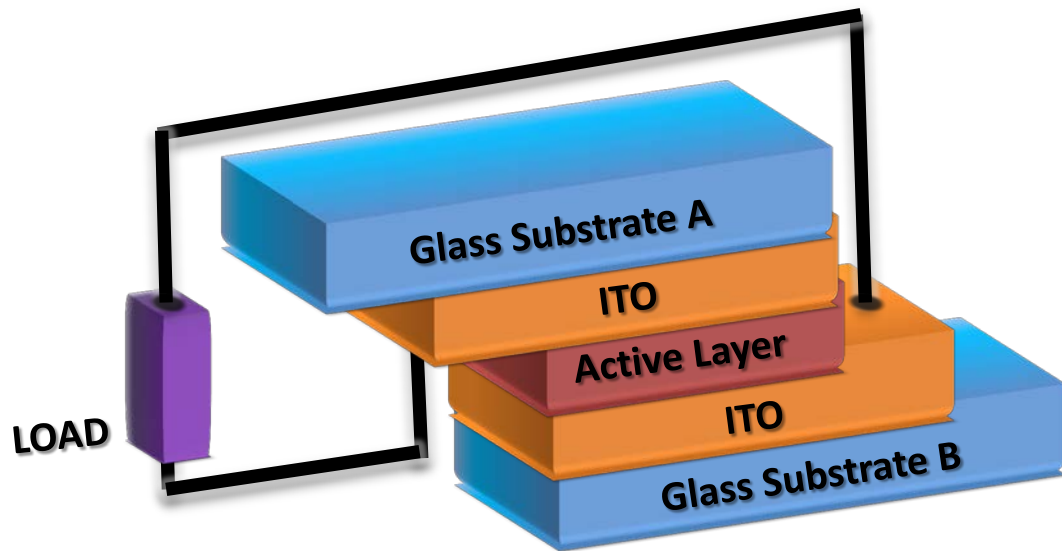
Figure 3.2 Device configuration of symmetrical electrode device

In a conventional organic photovoltaic device, a hole transport layer (PEDOT:PSS) is inserted in between ITO and active layer to improve anode contact. PEDOT:PSS is a typical P-type semiconductor, and usually worked as an electron-block layer. Thus, the insertion of PEDOT:PSS layers at both ITO electrodes of the symmetrical device would make it doesn't work due to the blockage of electron paths. However, a recent research by Dong et al. revealed that through Ultraviolet-ozone treatment, the PEDOT:PSS-free devices could reach identical and even higher efficiency compared with those devices with PEDOT:PSS. [63] In our experiment design, we adopted this PEDOT:PSS-free method to avoid the possible asymmetry caused by the deposition of PEDOT:PSS layer.

In general, the fabrication procedure of symmetrical device includes ITO

treatment, Thin film fabrication, Drying Process, and Thermal Annealing. All the steps

are done in a glove box filled with N_2. A brief summary of the manufacture procedure

is listed as follows:

a. ITO treatment: The patterned ITO/glass substrate (Thickness of ~150 Ohm,

    sheet resistance ~15 Ohm/cm^2) is pre-cleaned and treated with Ultraviolet

    (UV)-ozone plasma for 15 minutes before use.

b. Thin film fabrication: The blend of pre-dissolved P3HT and PCBM in DCB

    solution was added on the two ITO/glass substrates. Put the two substrates

    together. For the reference device 1 the PEDOT:PSS solution is used as the

    active layer while the ITO/glass substrates are directly put together in

    reference device 2.

c. Drying Process: The device was dried in DCB ambience for 2 to 3 hours.

    During the process, the device was kept flipping every 5 minutes to avoid the

    asymmetrical precipitation caused by gravity.

d. Thermal Annealing: The device was placed on a heating plate at 120°C for 10

    minutes.

e. Measurement: The as-made device then was put into a sealed glass container

    (jar) filled with inert N_2 during measurement. Two wires were connected with

    the electrodes through the plug of the jar.

3.2 Device characterizations

The organic photovoltaics are commonly evaluated by testing the Current-Voltage (I-V) characteristics. A I-V curve defines a relationship between the current through the device and the corresponding voltage across it. There are two methods to present the curves: Linear and semi-logarithmic representation as shown in **Figure** 3.3.
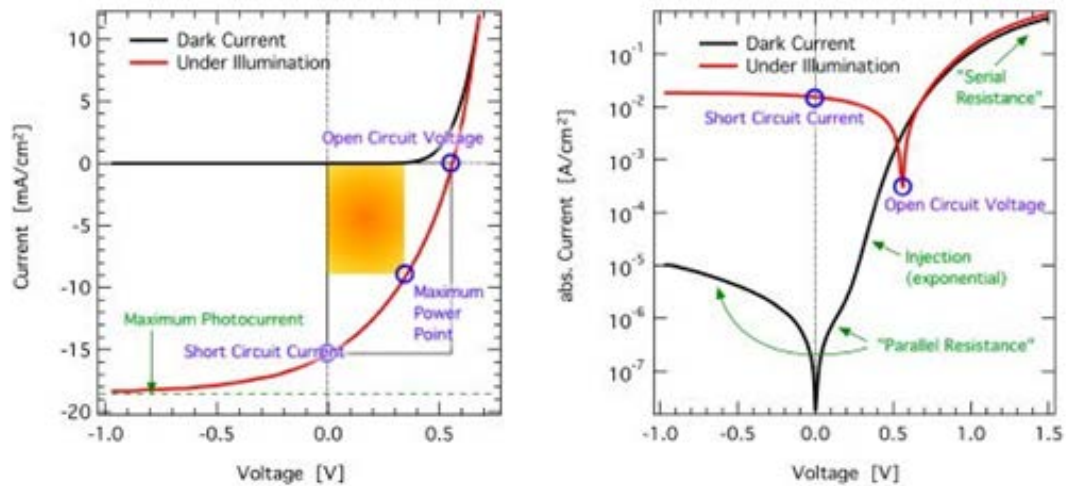
Figure 3.3 Linear and semi-logarithmic representation of current-voltage

characteristics for solar cells [45]

The I-V behavior is carried out under AM 1.5G illumination at 100 mW/cm^2 (SAN-EI Electric XEC-301S solar simulator, 300W Xe Lamp JIS Class AAA; beam size: 4 inch diameter). Through the measurement, we can obtain the information of open-circuit voltage (V_{oc}), short-circuit current (I_{sc}), fill factor (FF), and power

conversion efficiency (η).
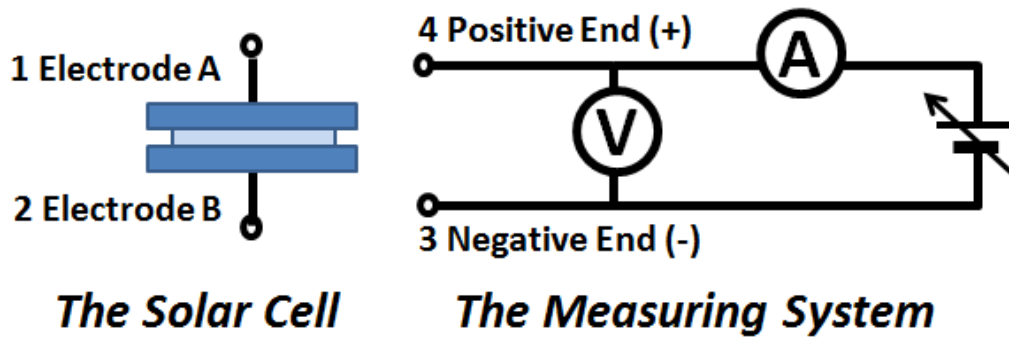
Figure 3.4 The measurement system for the current-voltage characteristics

Air mass (AM), a coefficient to describe the optical path length through the Earth's atmosphere, is an important parameter to characterize the solar cell performance under standardized conditions. The definition of AM is given as:

$$AM = \frac{1}{\cos z}$$

where z is the angle from the normal to the earth's surface (zenith angle). AM 1.5 is the mostly used environment for the efficiency measurement, where z is 48.2°.

For the better observation and analysis, we simplified the testing set-up (**Figure** 3.5). We position two lamps at the two opposite side of the device with a distance of 20 cm in the symmetrical measurement. The as-made device was put in a glass container filled with nitrogen. We can use the set-up to measure the photovoltaic behavior from either side illumination. The measurement parameters of each test

would be described in details in the results and discussion section.
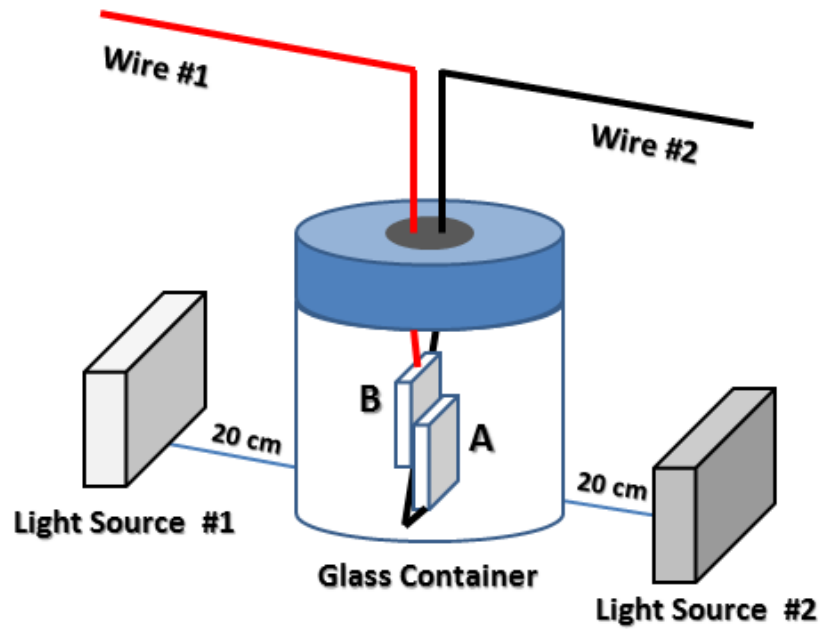
Figure 3.5 The set-up of the measurement system

Chapter 4 Results and Discussion

4.1 Hysteresis phenomenon in the devices

4.1.1 The reference devices

The symmetrical device employs two identical Indium Tin Oxide (ITO)/ glass substrates as the anode and cathode of the cell. Two referential cells named as reference device 1 and reference device 2 were made for comparison. The device configuration for reference 1 is ITO/PEDOT:PSS/ITO. For reference 2, two ITO electrodes were put together directly without an active layer sandwiched between (device structure: ITO/ITO).

We measured the devices with a scan rate of 20 mV/s and a voltage range from -1 V to 1 V. The obtained I-V curves are displayed in **Figure** 4.1. The reference 1 behaves as a constant resistor. The circuit of reference 2 is broken, since putting two ITO electrodes together directly provides a poor connection. The open-circuit characteristic of the reference 2 indicates that the I-V curves of reference 1 and the symmetrical device could not be caused by the short circuit of ITO electrodes.
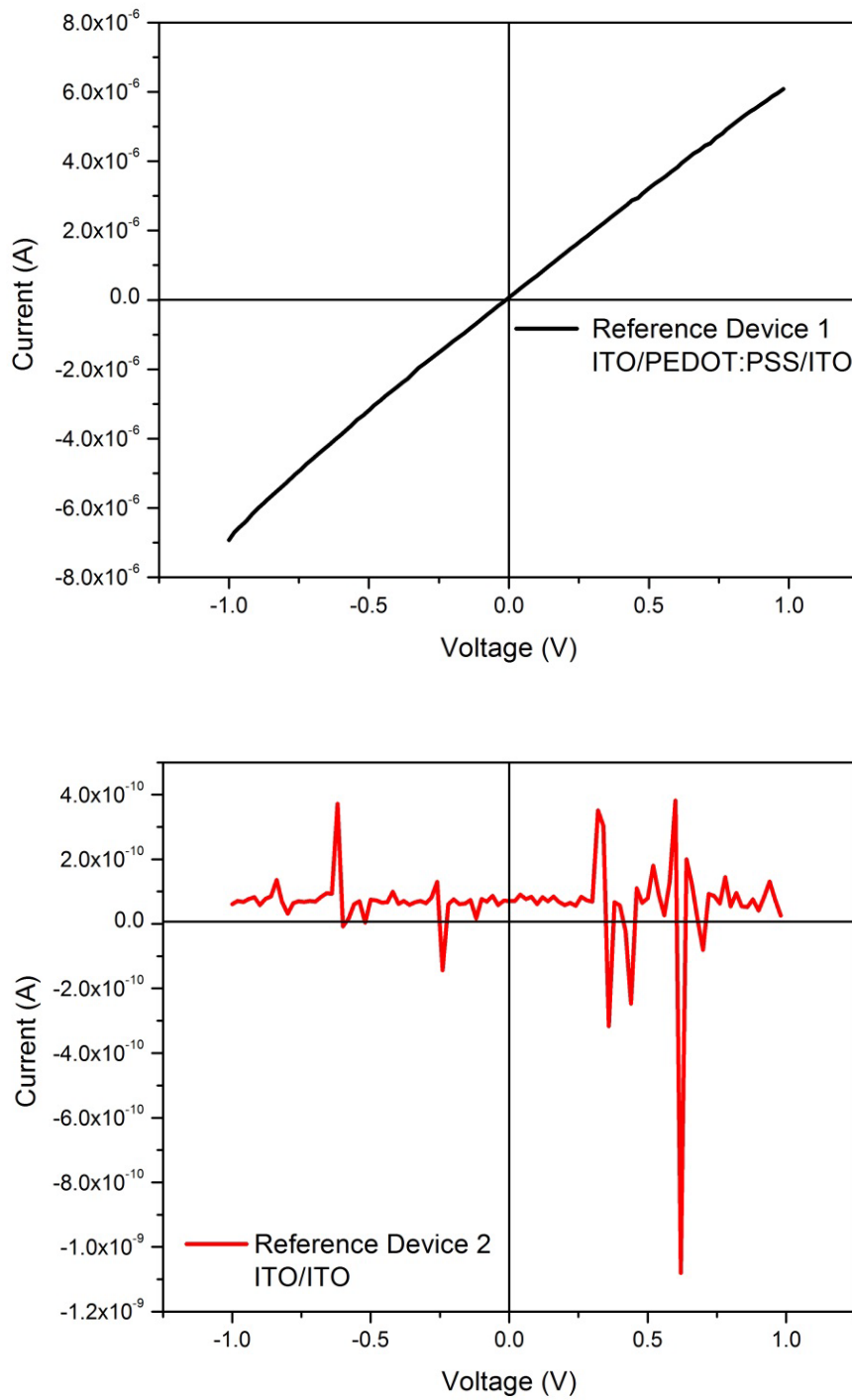
Figure 4.1 The I-V characteristics of reference device 1 and 2
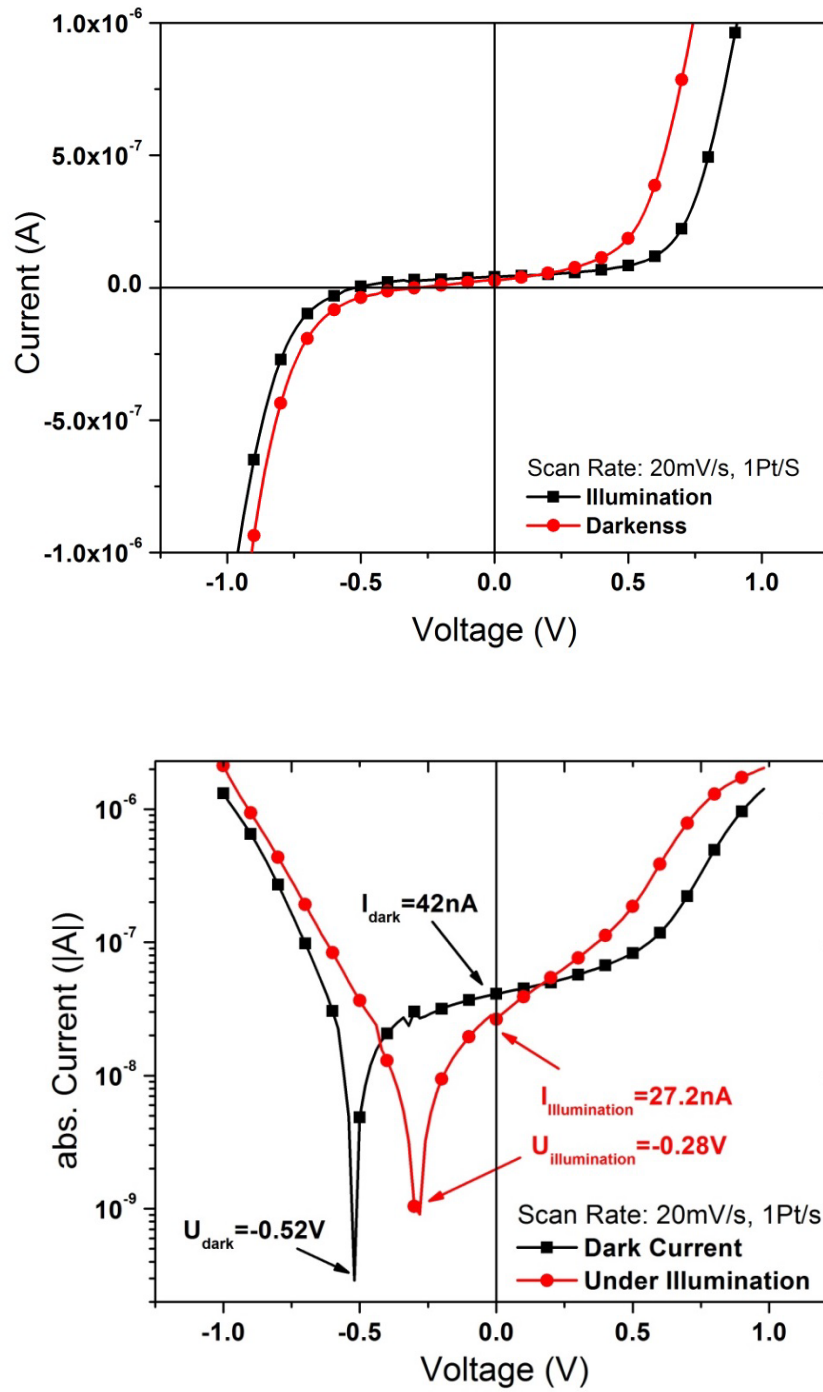
Figure 4.2 The I-V curves for the symmetrical device under illuminated and dark

condition

4.1.2 Asymmetrical performance from a symmetrical device

Figure 4.2 displayed the I-V curves of the symmetrical bulk heterojunction device under both illuminated and dark conditions. Surprisingly, it is found that such a symmetrical device exhibited asymmetrical behavior. In particular, it produces a non-zero open-circuit voltage, and a finite short-circuit current. The device has a large resistance of about 1 Mega Ohm, which is much larger than the common device.

According to the curve, the V_{oc} of the device is about 0.28 V under illumination. However, the open-circuit voltage (0.52 V) in the dark is abnormal to a solar cell. As we know, without photon absorption, no voltage could be produced by a solar cell in the dark. The dark voltage found in the I-V curves should be initiated by some unknown excitation during our experiment.

4.1.3 Possible causes of the asymmetry

In order to find the origin of the dark voltage, we start to confirm the deviation of our measurement system. We did the I-V measurement of three constant resistors (7.8 Mega Ohm, 23 Mega Ohm, and 2.3 Mega Ohm) at a slow scan rate (0.2 mV/s). The obtained I-V curves are exhibited in **Figure** 4.3. The three resistors comply with the Ohm's law and the deviations of the measurement system (crossover point of the three lines) are about 0.5 mV and 0.05 nA. The dark voltage could not be caused by the measurement system.

The electrodes could not be the cause either. Both the anode and the cathode are totally symmetrical since the two electrodes were cut from the same ITO/glass substrate and the treatments applied are identical.

It is difficult for the sandwiched device to keep both of the electrodes identical. During the preparation, we kept flipping the device every 5 minutes to avoid the asymmetrical precipitation caused by gravity. Therefore, the asymmetry of the electrodes is largely reduced and could not introduce the dark voltage.
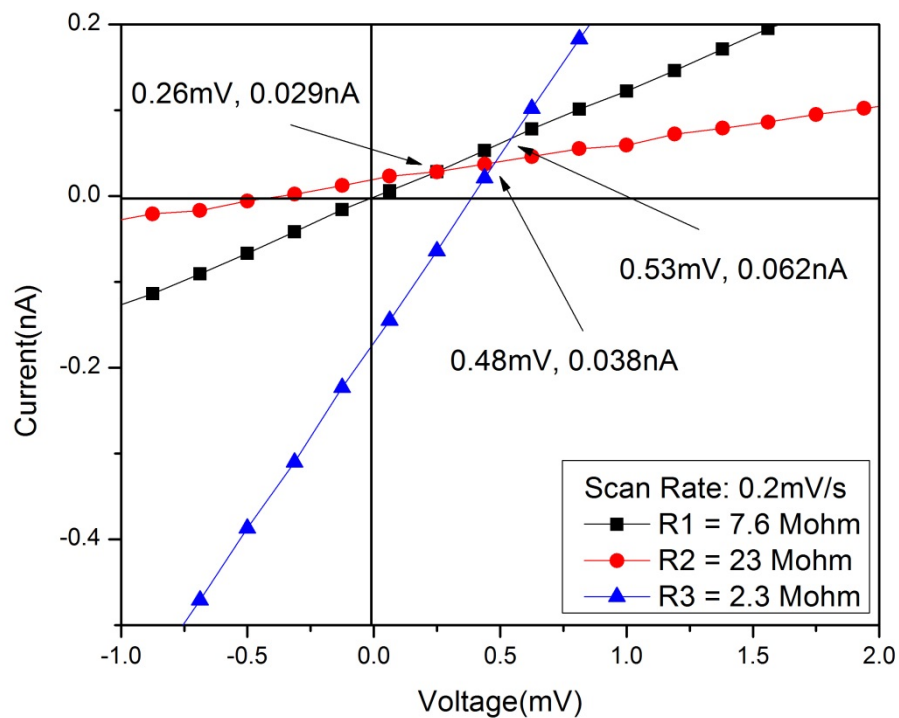
Figure 4.3 Experimental I-V curves for three constant resistors (7.6 Mega Ohm, 23 Mega Ohm, and 2.3 Mega Ohm)

It is found in literature that the initial measuring voltage might be the cause of the open-circuit voltage [65], but the following cyclic voltage scan results eliminated the possibility.

In a conventional device, the Aluminum and ITO electrodes are usually deposited in different way. The interface of Aluminum and active layer is easily damaged during the vacuum deposition. The differences between the deposition processes of the two electrodes might lead to an asymmetry. Alem et al. reported a symmetrical sandwiched device (Al/active layer/Al) could produce a voltage of 0.15 V, which is attributed to the different top and bottom electrode interface. [64] The two Al electrode interfaces are formed under different environments: the later deposited metal films could introduce thermal damage to the active layer surface during the deposition while there is no interfacial damage caused by the early deposited metal layer. However, the method we used causes no damage in electrode interfaces.

4.1.4 Cyclic voltage scan results

To unveil the mystery of the dark voltage, we did the cyclic voltage scan (CV) measurement. We found that the dark voltage started to change its sign when the voltage scanned from the opposite direction as shown in **Figure** 4.4.

The dark voltage might be caused by the hysteresis phenomenon in the device.

The p/n junction or the acceptor/donor interface in the bulk heterojunction could be considered as an intrinsic capacitor.
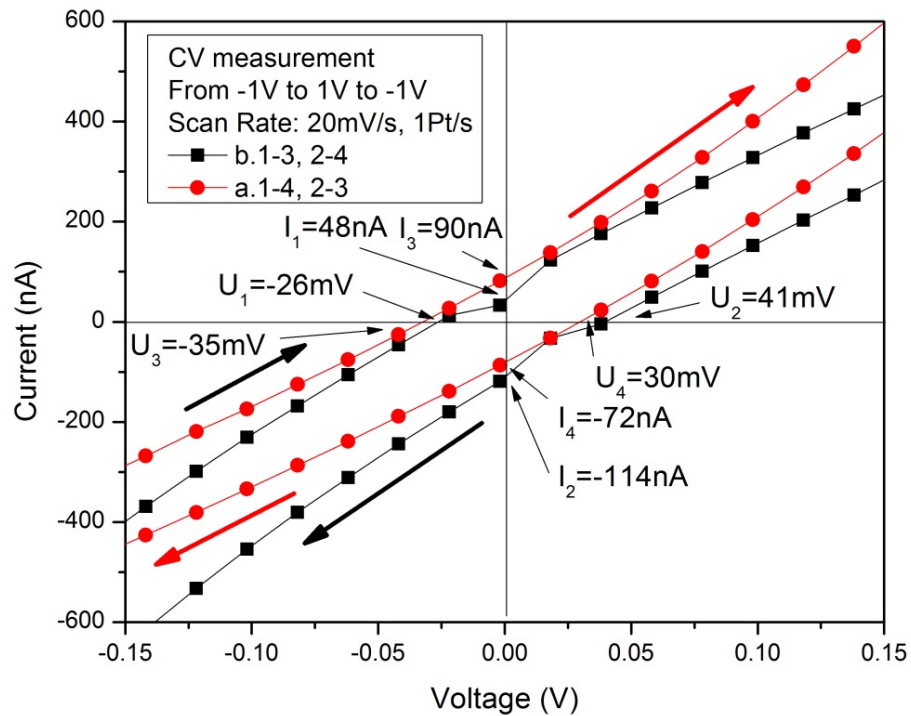
Figure 4.4 The cyclic voltage scan of the symmetrical device

The time constant (τ) of a capacitor is given by:

$$\tau = R \times C$$

where R is the resistance, and C the capacitance of the device.

The hysteresis appears when the time constant is smaller than the total scan time. The large time constant of the device is caused by the resistance of 1 Mega Ohm,

57

which is thousands of times larger than that of a normal organic solar cell.
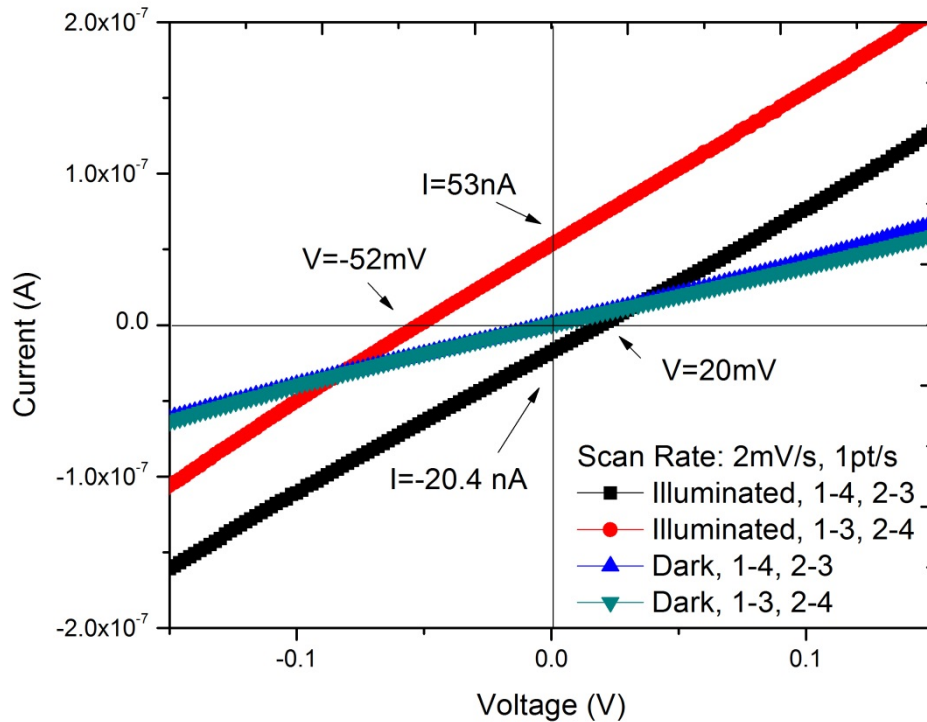
Figure 4.5 The slow scan rate I-V results under illumination and in the dark

We reduced the scan rate from 20 mV/s to a much slower one (2 mV/s) and re-measure the device. The I-V curves are shown in **Figure** 4.5. As indicated before (**Figure** 3.3), the 1 and 2 refer to the A side and B side electrode of the device, and 3 and 4 represent the negative and positive end of measuring power. According to the curves, the dark voltage has been removed. To our surprise, the asymmetry still exists in the device under illumination. Even when we change the wiring direction of the

device (scan voltage: from -1 V to 1 V), the sign of the open circuit voltage for the symmetrical device keeps unchanged (20 mV for the black square line and 52 mV for the red dot line).

4.2 Asymmetric I-V behavior polarized by illumination

It is common sense that we can only obtain the symmetrical results when measuring a symmetrical device. The symmetrical device could not produce current since both of the electrode interfaces are identical. Asymmetry must exist in either fabrication or measurement. The only possible asymmetry is caused by the illumination.
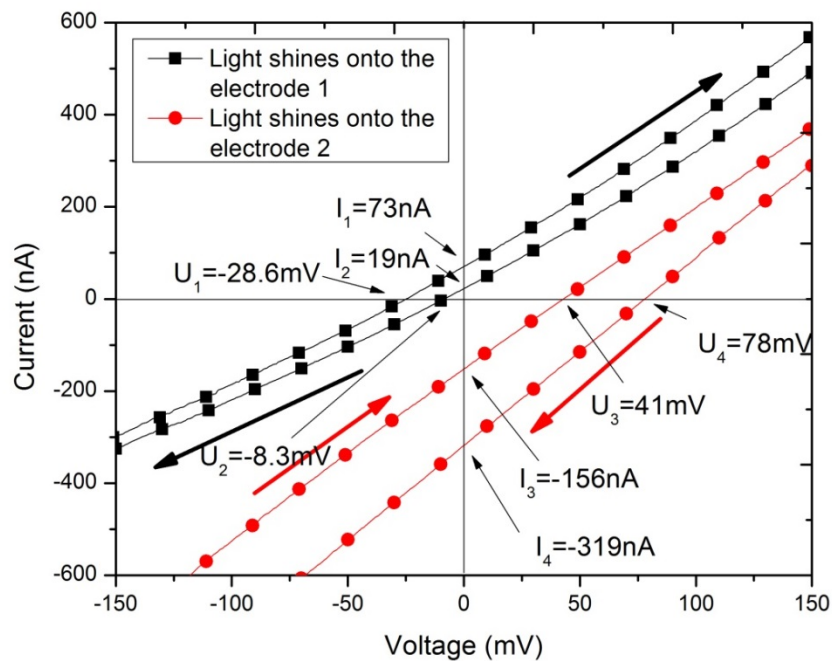
Figure 4.6 The I-V curves of the device under different illumination condition

(electrode 1 and 2 refer to the side A and B of the device as shown in **Figure** 3.3)

The estimated thickness of the symmetrical device is 100 micrometers, while 100 nanometers is sufficient for the photon absorption. The exciton could be generated only in the vicinity of the electrode illuminated. In the region near the other electrode (dark electrode), few excitons could be created. For the organic semiconductor, the diffusion length for the exciton is rather small, at about 10 nm. Thus, the separated charge carriers are all accumulated in the exciton generation regions.

To verify the asymmetry of illumination, we measure the I-V characteristics of the device using different illumination direction (electrode 1 and electrode 2). As shown in **Figure** 4.6, the open-circuit voltage is -28.6 mV when the illuminated electrode is electrode 1 (side A in **Figure** 3.3), while 78 mV for illumination on electrode 2 (side B in **Figure** 3.3). The results validate that the asymmetry is due to the illumination.

4.3 Equivalent circuit analysis

As shown in **Figure** 4.7, the I-V curves in the dark are symmetrical about the origin. The small deviation at the origin is caused by the fabrication errors, and could be avoided.
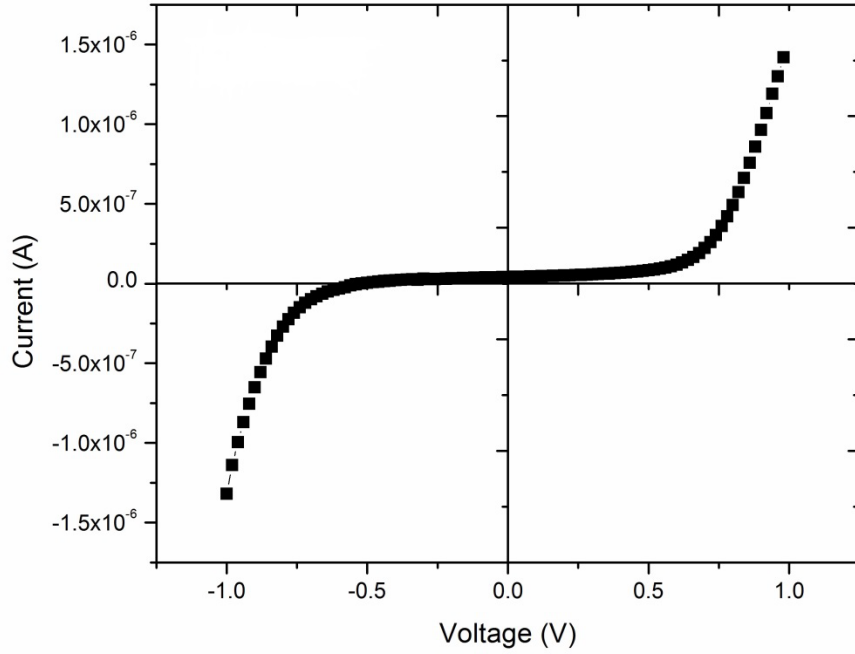
Figure 4.7 The I-V curve of the symmetrical device in the dark
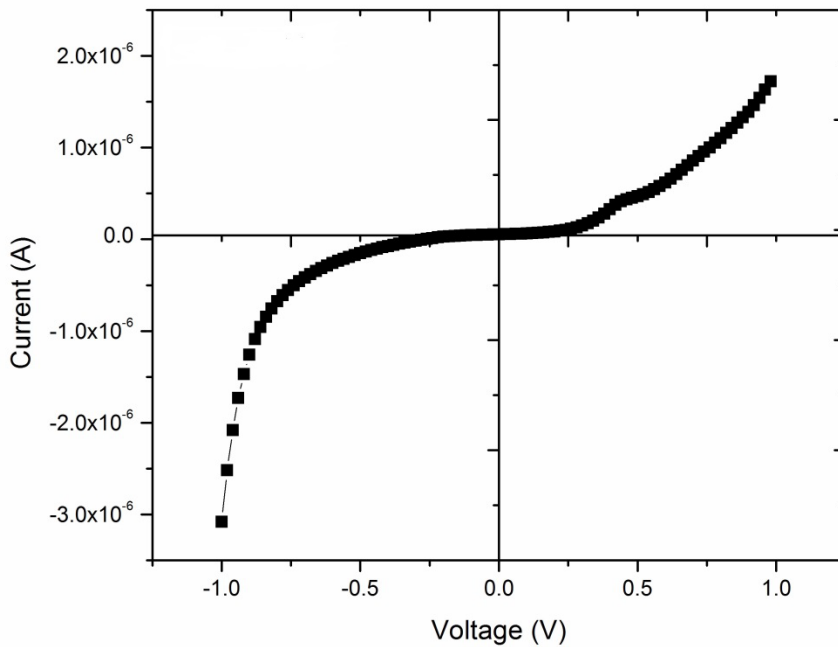
Figure 4.8 The I-V curve of the symmetrical device under illumination

The asymmetrical I-V curve indicates the equivalent circuit of the symmetrical device should include two identical diodes connected in opposite direction. Only by parallel connection could the device present such I-V characteristics. When illuminated, the I-V curves become asymmetrical as exhibited in **Figure** 4.8. The illuminated electrode is the cathode (negative side).

We assumed there is a vertical phase segregation in bulk Heterojunction layer, which is attributed to the differences in the surface energy of P3HT (27.2 mN/m) and PCBM (38.2 mN/m) [66]. The vertical phase segregation in BHJ had been observed by several groups [57, 67]. Since PCBM has a higher surface energy than P3HT, it may tend to accumulate at the ITO substrate to reduce the overall energy. During the fabrication of the device, we added the blend layer on two ITO substrates separately and then put them together. Thus, we assume that the P3HT is distributed in the middle part of the active layer while the domain near the ITO electrode is likely comprised of PCBM. The proposed structure is displayed in **Figure** 4.9.

When the exciton dissociated at the region near the electrode illuminated, the electrons as well as holes would diffuse to the illuminated electrode. Since the PCBM has a much larger interface area with the electrode, the illuminated electrode works as the cathode, while the dark electrode becomes the anode. The equivalent circuit for the symmetrical device is exhibited in **Figure** 4.10.
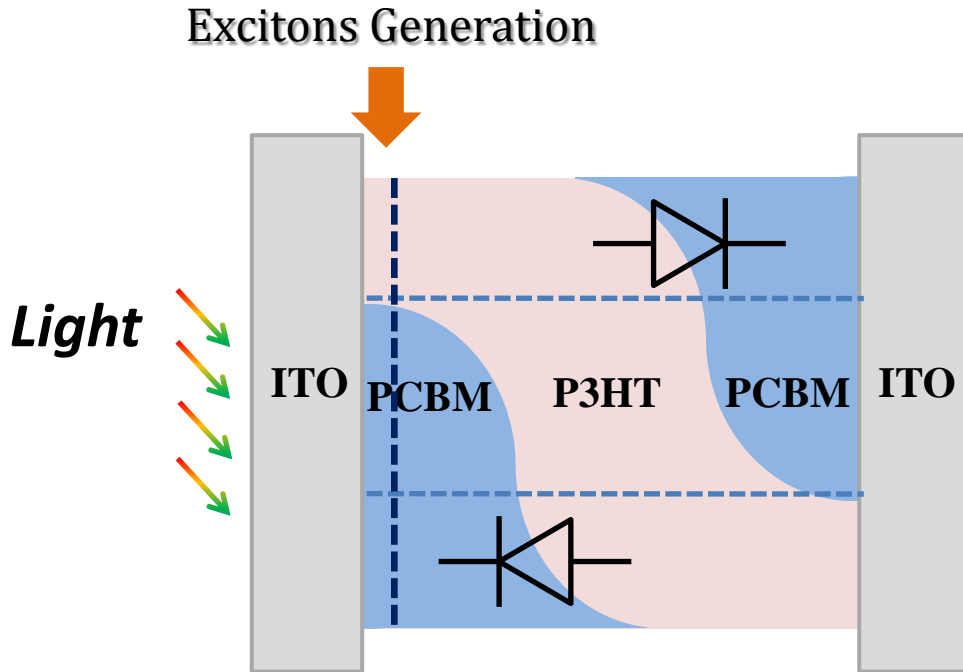
Figure 4.9 The proposed structure of the symmetrical device

Because of the asymmetry of exciton absorption, only one current source could work under illumination. Assuming the working current source is j_{sc1}, the device will exhibit the photovoltaic characteristics due to D_1 for forward bias condition. Under reverse bias, the D_2 starts to work and an anti-symmetrical current-voltage behavior will be displayed.

The diode equation for the device [61] could be modified as:

$$j(V) = -j_1 \left\{ exp \left\{ \frac{q(jR_s - V)}{n_1 kT} \right\} - 1 \right\} + j_2 \left\{ exp \left\{ \frac{q(V - jR_s)}{n_2 kT} \right\} - 1 \right\}$$

$$-\frac{V - jR_s}{R_{sh}} + j_{sc1} - j_{sc2}$$

where j_1 and j_2 is the saturation current density of diode 1 and diode 2, n_1 and n_2 the ideality factor of diode 1 and diode 2, q the elementary charge, KT the thermal energy, R_s the series resistance, R_{sh} the shunt resistance of the device, j_{sc1} and j_{sc2} the photocurrent of current source 1 and 2.
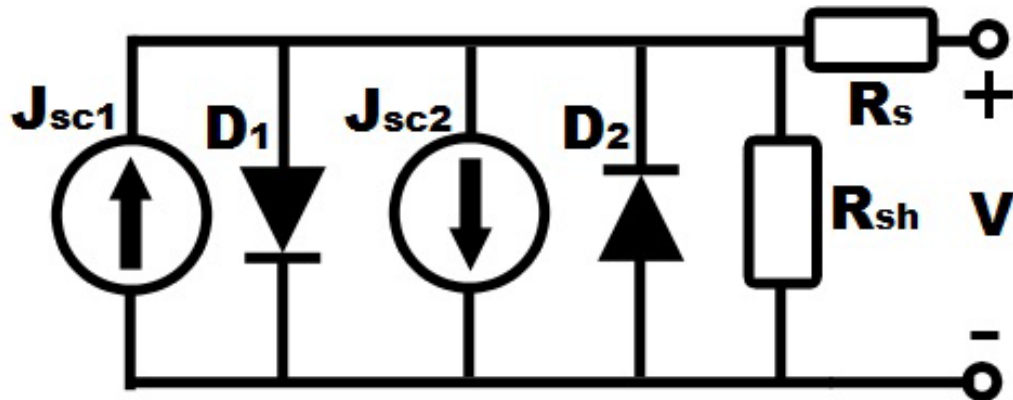
Figure 4.10 The equivalent circuit for the symmetrical device

Three different types of symmetrical photovoltaic device were reported recently, as shown in **Figure** 4.11. However, the effect of illumination could only be observed in our device. The active layer thickness of both the planar ITO device [65] and planar Al device [68] is too small, and no difference would be formed in the exciton generation. The output voltage of sandwiched Al device [64] is caused by the

asymmetrical electrode interfaces. Thus, the sandwiched ITO device could be the only choice to unveil the asymmetry of illumination.
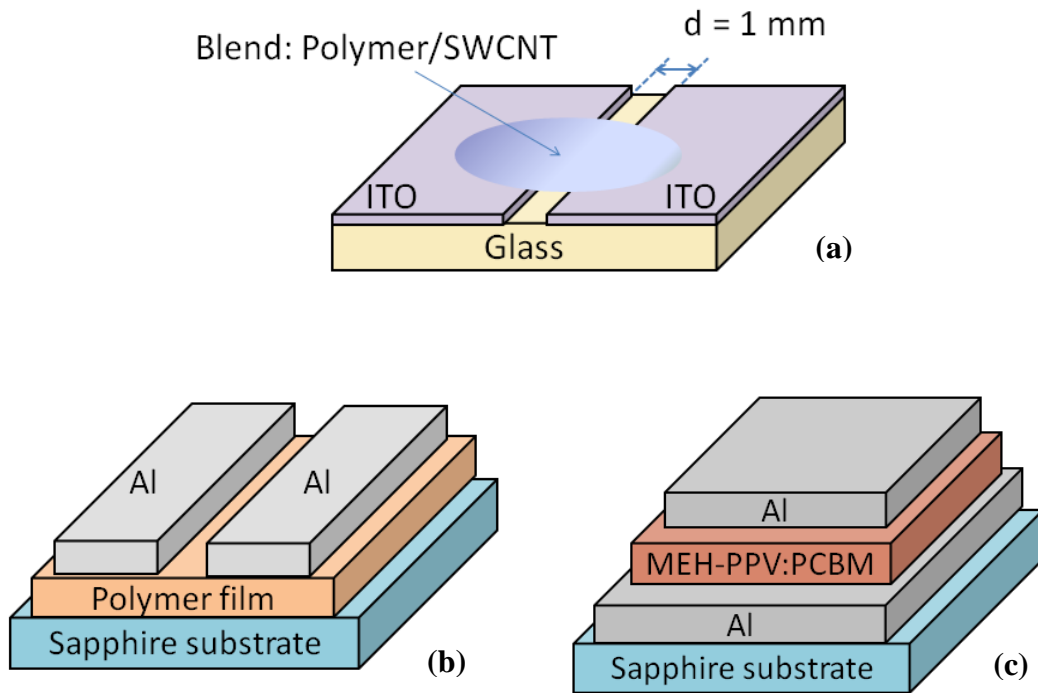
Figure 4.11 Three typical symmetrical devices in literature: (a) planar ITO device; (b) planar Al device; (c) sandwiched Al device

The proposed equivalent circuit model could be used to explain the I-V characteristics of our device. However, some key issues such as the charge transport processes in the active layer remain unknown. The energy diagram is needed for further exploration of the operation mechanism of the symmetrical devices.

4.4 Energy diagram analysis

The energy diagram is the most important tool to analyze the operation mechanism of solar cells. M-i-M model (**Figure** 2.9) and p-type Schottky Junction model (**Figure** 2.10) are two commonly used models for energy diagram of bulk heterojunction organic solar cells. However, both of them are flawed.

4.4.1 Two dominating energy diagram models

M-i-M model originates from the M-i-M structure. M-i-M model had been widely employed in explanation of the device physics of bulk heterojunction organic solar cells, such as the origin of output voltage and the driving force for the charge separation. However, the model is based on the two inappropriate assumptions: the organic layer is an insulator and the thickness of the layer is less than 10 nanometers.

According to the model, the symmetrical device could not work since the work function difference between the two electrodes is zero (shown in **Figure** 4.12). The output voltage produced in our symmetrical device proves that the M-i-M model is not applicable to the symmetrical BHJ devices.

The p-type Schottky Junction model is a newly proposed model based on experimental results [54]. The model is successful in explaining the charge carrier

distribution, transport properties, and lifetime in the bulk heterojunction. Despite its wide application, the p-type Schottky Junction model is self-contradicted to some extent. For example, it is unreasonable that the p-type semiconductor, which is a hole transport layer, could be used to transport electrons.
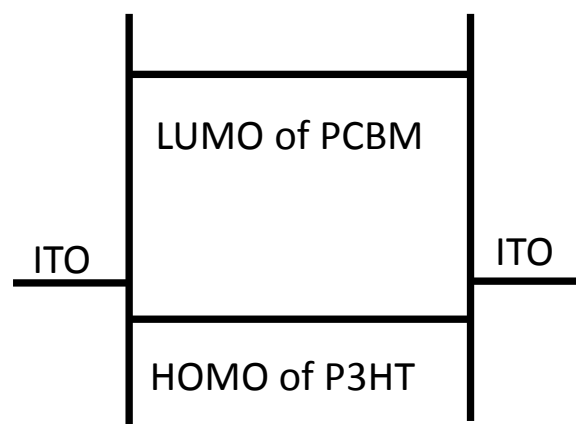
M-i-M model
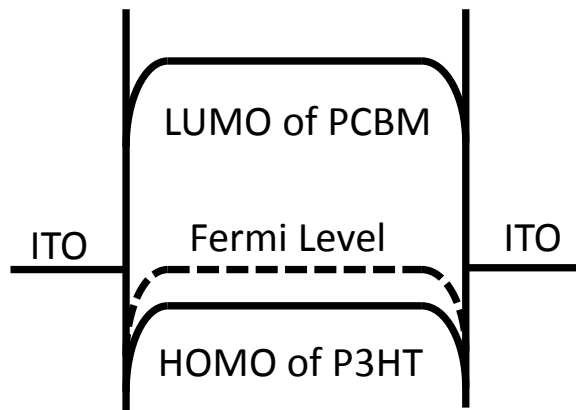
P-type Schottky Junction model

Figure 4.12 The energy diagram of the symmetrical device in the M-i-M model and the P-type Schottky Junction model

The energy diagrams of the symmetrical device in the M-i-M model and the p-type Schottky Junction model are shown in **Figure** 4.12. The energy diagram in the p-type Schottky Junction model is symmetrical, and thus the barriers to the charge carriers are identical at both electrode interfaces. A DC current couldn't be formed and no photovoltaic performance would be displayed. However, it is opposite to our results.

Therefore, to explain the symmetrical device, a new model is needed.

4.4.2 The proposed model

In our device, three interfaces exist, i.e. P3HT/ITO, PCBM/ITO, and P3HT/PCBM interface. The P3HT and PCBM in the active layer are equally distributed and their respective agglomeration domain sizes are 5 to 10 nanometers. [69] And the energy levels of the materials for BHJ device are shown in **Figure** 4.13.
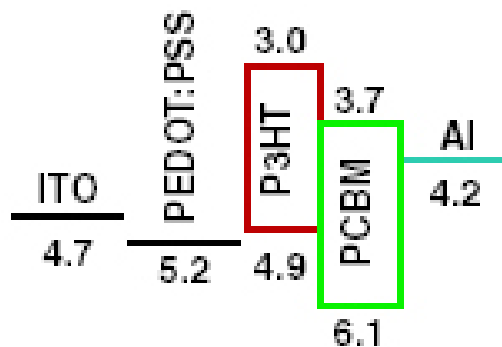
Figure 4.13 Energy levels of the materials for BHJ device
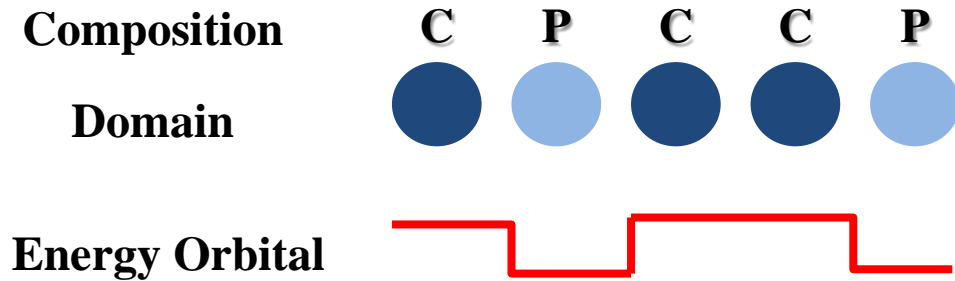
Figure 4.14 The energy diagram of the bulk heterojunction (P refers to P3HT and C

represents PCBM)

Due to few space charges accumulated in the P3HT or PCBM region, very

small or nearly no band bending exists at the interfaces. The holes in P3HT and

electrons in PCBM are transported in different manner: the holes favor higher energy

levels (for electrons) while the electrons would like to move towards low energy

levels. The Energy orbital of P3HT (HOMO) is lower than that of PCBM (LUMO).

The transport path for a charge carrier is exhibited in **Figure** 4.14. The output voltage

would be the potential difference between initial state (C) and final state (P). In fact,

the paths for charge carriers in bulk heterojunction are much more complicated with

more interfaces.

The actual microstructure of bulk heterojunction could be considered as a

mixture of spaghetti for P3HT polymer and meatballs for PCBM (shown in **Figure**

4.15). Thus, the former assumption of bulk heterojunction in **Figure** 4.9 is incorrect.

P3HT is a long chain polymer while PCBM is a fullerene derivative. The two are well distributed and interpenetrated in the layer. The path for charge carrier's transport could be taken of as a sequence with different number of elements (P3HT or PCBM) and in multifarious orders. There are many paralleled paths between the two electrodes.
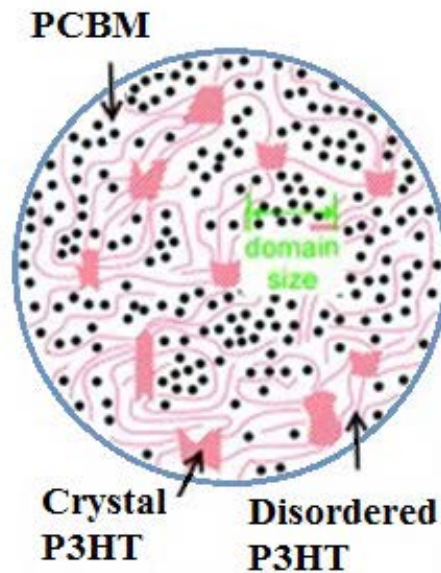
Figure 4.15 The microstructure of bulk heterojunction

For simplification, the blend model of simple 5-position path is analyzed. A much more complex system with more positions could also be considered as a 5-position system because some positions could be considered as repeating of the 5-position system.

Since each position of the 5-position path could only be occupied by either P

(P3HT) or C (PCBM), there are 32 paths for the BHJ structure. To produce an output

voltage, the final position and the initial position should be different. Therefore, only

16 of them are possible for transport of charge carriers (from the left side to the right

side in **Figure** 4.16).
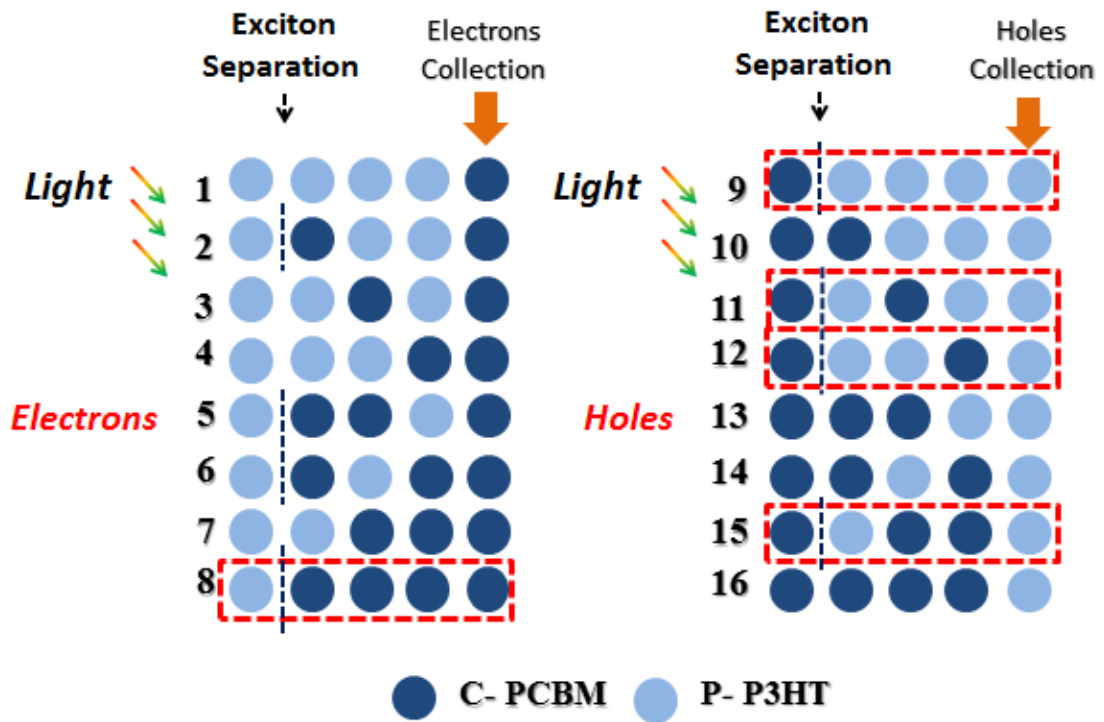
Figure 4.16 The possible charge transport paths for charge carriers

P3HT is a well-spread long chain polymer and the holes can hop through the

PCBM barrier from one P3HT position to another (**Figure** 4.17). However, the

situation for the electron is different. Since the PCBM is accumulated in isolated

regions, the electron could not transport through the barrier of P3HT. Therefore, only one path is effective for the electrons and four for the holes, which are all indicated by the red dotted boxes in **Figure** 4.16.
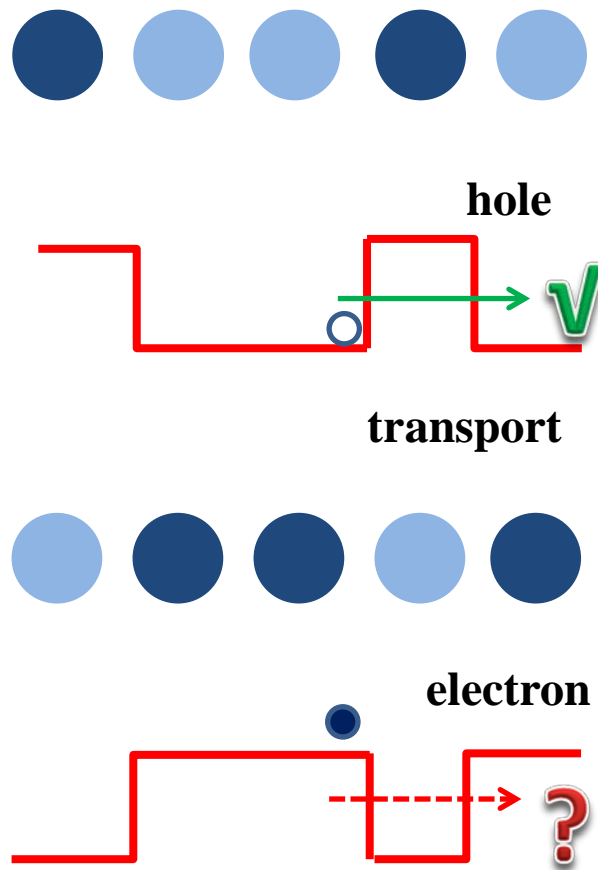
Figure 4.17 The charge carrier transport paths

Under illumination, most of the holes are transported to the dark electrodes while the electrons would be collected by the illuminated electrode directly. The final dynamic equilibrium between the holes and electrons movement produces a DC

current. The long distance transport results in the large resistance and small short-circuit current of the device.

In summary, the photovoltaic performance is resulted from the asymmetrical exciton distribution by the asymmetrical illumination. The interpenetrated structure of P3HT and PCBM makes it easier for the holes to be transported to the dark electrode, while the electrons could only be extracted by the illuminated electrode. The equivalent circuit of the device is a pair of inversely paralleled diodes.

Chapter 5 Conclusion

As a promising candidate to silicon-based solar cells, the organic photovoltaic is attractive due to the cost advantage and mechanical flexibility. A huge development has been made during last 30 years, including the understanding of the device physics, the stability enhancement, and the efficiency improvement. However, some key issues in the device physics of the organic photovoltaics remain unsolved, such as controversy on the widely used energy diagrams.

In the thesis, a symmetrical structure is introduced to explore the controversy. We want to isolate the asymmetry of the materials and device from the symmetrical structure. Surprisingly, the symmetrical device produces a non-zero open-circuit voltage and a finite current. The performance was found to be caused by the asymmetrical illumination and the illuminated electrode turn out to be the cathode. The photovoltaic behavior of the symmetrical device effectively invalidates the widely used M-i-M model and P-type Schottky Junction model, both of which predict that the symmetrical BHJ devices could not work.

The equivalent circuit of inverse parallel diodes as well as a new model for the

bulk heterojunction energy diagram is proposed to explain the observed characteristics and understand the operation mechanism of the symmetrical device, which would certainly have a profound influence in the manufacture method as well as the device physics analysis of bulk heterojunction organic photovoltaics.

Bibliography

[1] BP Statistical Review of World Energy June 2013. BP

[2] S. Shafiee, and E. Topal, "When will fossil fuel reserves be diminished?", *Energy Policy*, 2009, **37**, 181.

[3] Renewable Energy.

http://au.pfinance.yahoo.com/compare/energy/faqs/renewable-energy/

[4] The Growing Need for Renewable Energy. Gilberto Galea. September 26, 2013.

http://greenliving4live.com/2013/09/growing-need-renewable-energy/

[5] Hydroelectric Energy Generation.

http://www.efficientgreenpower.com/hydroelectric-energy

[6] Wikimedia - Nesjavellir Power Plant.

http://en.wikipedia.org/wiki/File:NesjavellirPowerPlant_edit2.jpg

[7] The Renewables 2011 Global Status Report. http://www.ren21.net.

[8] BP Statistical Review of World Energy 2011. BP.

[9] Wikimedia-Solar Radiation Spectrum.

http://commons.wikimedia.org/wiki/File:Solar_Spectrum.png

[10] Science: Archimedes' Weapon, Time magazine.

http://content.time.com/time/magazine/article/0,9171,908175,00.html?promoid=googl ep.

[11] A. E. Becquerel, "Recherches sur les effets de la radiation chimique de la lumiere solaire au moyen des courants electriques", *Comptes Rendus de L'Academie des Sciences*, 1839, **9**, 145.

[12] M. A. Green, "Photovoltaics: coming of age", *21st IEEE Photovoltaic Specialists Conference, Kissimimee*, May, 1990, 1.

[13] P. Gevorkian, "Sustainable energy systems engineering: the complete green building design resource", *McGraw-Hill Professional*.

[14] "The Nobel Prize in Physics 1921: Albert Einstein", Nobel Prize Official Page. http://www.nobelprize.org/nobel_prizes/physics/laureates/1921/

[15] M. Riordan, and L. Hoddeson. "The origins of the pn junction", *IEEE Spectrum*, June, 1997, 46.

[16] R. Ohl, "Light-sensitive electric device including silicon" US Patent 2443542 A. June 15, 1948.

[17] D. Chapin, C. Fuller, G. Pearson, " A New Silicon p-n Junction Photocell for Converting solar Radiation into Electrical Power", *Journal of Applied Physics*, 1954, **25**, 676.

[18] I. Dharmadasa, "Advances in Thin-Film Solar Cells", *CR Press*, 2012.

[19] The History of Solar Power.

http://www.homesolarinfo.com/the-history-of-solar-power.html

[20] X. Wu, J. Kane, R. Dhere, C. Dehart, D. Albin, A. Duda, T. Gessert, S. Asher, D. Levi, and P. Sheldon, "16.5% Efficiency CdS/CdTe polycrystalline thin-film solar cells", *Proceedings of the 17th European Photovoltaic Solar Energy Conference and Exhibition, Munich*, 2002, 995.

[21] K. Ramanathan, M. Contreras, C. Perkins, S. Asher, F. Hasoon, J. Keane, D. Young, M. Romero, W. Metzger, R. Noufi, J. Ward, and A. Duda, "Properties of 19.2% efficiency ZnO/CdS/Cu(In, Ga)Se$_2$ thin-film solar cells", *Progress in Photovoltaics: Research and Applications*, 1999, **11**, 225.

[22] Information about First Solar Cell. http://www.firstsolar.com/About-First-Solar

[23] Which Thin Film Solar Technology is the Best?

http://www.solar-facts-and-advice.com/thin-film.html

[24] J. Zhao, A. Wang, M. Green, F. Ferrazza, "19.8% efficient 'honeycomb' textured multicrystalline and 24.4% monocrystalline silicon solar cells", *Applied Physics Letters*, 1998, **73**, 1991.

[25]W. Shockley, and H. Queisser, "Detailed Balance Limit of Efficiency of p-n Junction Solar Cells", *Journal of Applied Physics*, 1961, **32**, 510.

[26] Generation Gap of Solar Cell.

http://environmentalresearchweb.org/cws/article/news/30489/1/Generationgap

[27] R. Schaller, and V. Klimov, "High Efficiency Carrier Multiplication in PbSe

Nanocrystals Implications for Solar Energy Conversion", *Physical Review Letters*, 2004, **92**, 196601.

[28] Quantum Dots May Boost Photovoltaic Efficiency to 65%.

http://www.futurepundit.com/archives/002789.html

[29]Invention of DSSC.

https://workspace.imperial.ac.uk/people/Public/chemistry/Brian%20ORegan/EarlyHistory.html

[30] B. O'Regan, and M. Gratzel, "A low-cost, high-efficiency solar cell based on dye-sensitized colloidal TiO$_2$ films", *Nature*, 1991, **353**, 737.

[31] I. Chung, B. Lee, J. He, R. Chang, and M. Kanatzidis, "All-Solid-State Dye-Sensitized Solar Cells with High Efficiency", *Nature*, 2012, **485**, 4886.

[32] D. Kearns, and M. Calvin, "Photovoltaic effect and photoconductivity in organic laminated systems", *Journal of Chemical Physics*, 1958, **29**, 950.

[33] C. W. Tang, "Two-layer organic photovoltaic cell", *Applied Physics Letters*, 1986, **48**, 183.

[34] G. Yu, J. Gao, J. Hummelen, F. Wudl, and A. Heeger, Polymer photovoltaic cells - enhanced efficiencies via a network of internal donor-acceptor heterojunctions, *Science*, 1995, **270**, 1789.

[35] Heliatek, Heliatek and AGC sign a development agreement to integrate organic solar films in glass.

http://www.agc-glass.eu/English/Homepage/News/Press-room/Press-Detail-Page/page .aspx/979?pressitemid=3202

[36] T. Ameri, G. Dennler, C. Lungenschmied, and C. Brabec, "Organic tandem solar cells: A review", *Energy and Environmental Science*, 2009, **2**, 347.

[37] National Renewable Energy Laboratory, US Department of Energy, Best Research Photovoltaic Cell Efficiencies, 2013. (http://www.nrel.gov/pv/)

[38] J. Nelson, "Polymer:fullerene bulk heterojunction solar cells", *Materials Today*, 2011, **14**, 462.

[39] D. Muhlbacher, M. Scharber, M. Morana, Z. Zhu, D. Waller, R. Gaudiana, and C. Brabec, "High Photovoltaic Performance of a Low-Bandgap Polymer", *Advanced Materials*, 2006, **18**, 2884.

[40] B. Eliasson, "Metal-Insulator-Metal Diodes for Solar Energy Conversion", Ph.D Dessertation, University of Colorado, 2001.

[41] T. Kirchartz, K. Taretto, and U. Rau, "Efficient Limits of Organic Bulk Heterojunction Solar Cells", *Journal of Physics C*, 2009, **113**, 17958.

[42] Introduction to Conventional Solar Cells.

http://www.haverford.edu/kinsc/boe/dssc/

[43] D. Demeo, S. MacNaughton, S. Sonkusale, and Vandervelde, "Chapter 7: Electrodeposited Copper Oxide and Zinc Oxide Core-Shell Nanowire Photovoltaic Cells", *Nanowires - Implementations and Applications*, 2011.

[44] S. Dimitrijev, "Principles of Semiconductor Devices (Second Edition)", *Oxford University Press, New York,* 2012.

[45] C. Deibel, and V. Dyakonov, "Polymer-fullerene bulk heterojunction solar cells", *Reports on Progress in Physics*, 2010, **73**, 096401.

[46] W. Ma, C. Yang, X. Gong, K. Lee, and A. Heeger, "Thermally Stable, Efficient Polymer Solar Cells with Nanoscale Control of the Interpenetrating Network Morphology", *Advanced Functional Materials*, 2005, **15**, 1617.

[47] G. Chamberlain, "Organic solar cells: A review", *Solar Cells*, 1983, **8**, 47.

[48] J. Liu, Y. Shi, and Y. Yang, "Solvation-induced Morphology Effects on the Performance of Polymer-Based Photovoltaic Devices", *Advanced Functional Materials*, 2001, **11**, 420.

[49] M. Scharber, D. Muhlbacher, M. Koppe, P. Denk, C. Waldauf, A. Heeger, and C. Brabec, "Design Rules for Donors in Bulk-Heterojunction Solar Cells - Towards 10% Energy-Conversion Efficiency", *Advanced Materials*, 2006, **18**, 789.

[50] R. Loutfy, J. Sharp, C. Hsiao, and R. Ho, "Phthalocyanine organic solar cells: Indium/x-metal free phthalocyanine Schottky barriers", *Journal of Applied Physics*, 1981, **52**, 5218.

[51] T. Stubinger, and W. Brutting, "Exciton diffusion and optical interference in organic donor-acceptor photovoltaic cells", *Journal of Applied Physics*, 2001, **90**, 3632.

[52] A. Tada, Y. Geng, Q. Wei, K. Hashimoto, and K. Tajima, "Tailoring organic heterojunction interfaces in bilayer polymer photovoltaic devices", *Nature Materials*, 2011, **10**, 450.

[53] H. Hoppe, and N. Sariciftci, "Organic solar cells: An overview", *Journal of Materials Research*, 2004, **19**, 1924.

[54] J. Bisquert, and G. Garcia-Belmonte, "On Voltage, Photovoltage, and Photocurrent in Bulk Heterojunction Organic Solar Cells", *Journal of Physical Chemistry Letters*, 2011, **2**, 1950.

[55] Y. Kim, S. Choulis, J. Nelson, D. Donal, S. Cook, and J. Durrant, "Device annealing effect in organic solar cells with blends of regioregular poly(3-hexylthiophene) and soluble fullerene", *Applied Physics Letters*, 2005, **86**, 063502.

[56] Y. Zhao, Z. Xie, Y. Qu, Y. Geng, and L. Wang, "Solvent-vapor treatment induced performance enhancement of poly(3-hexylthiophene_: methanofullerene bulk-heterojunction photovoltaic cells", *Applied Physics Letter*, 2007, **90**, 043504.

[57] Z. Xu, L. Chen, G. Yang, C. Huang, J. Hou, Y. Wu, G. Li, C. Hsu, and Y. Yang, "Vertical Phase Separation in Poly(3-hexylthiophene): Fullerene Derivative Blends and its Advantage for Inverted Structure Solar Cells", *Advanced Functional Materials*, 2009, **19**, 1227.

[58] M. Drees, K. Premaratne, W. Graupner, J. Helfin, R. Davis, D. Marciu, and M.

Miller, "Creation of a gradient polymer-fullerene interface in photovoltaic devices by thermally controlled interdiffusion", *Applied Physics Letters*, 2002, **81**, 4607.

[59] N. Yeh, and P. Yeh, "Organic solar cells: Their developments and potentials", *Renewable and Sustainable Energy Reviews*, 2013, **21**, 421.

[60] K. Wang, "Nanomaterials: from Interfacial Characteristics to Device Applications", Ph.D Dissertation, McMaster University, 2011.

[61] J. Nelson, "The Physics of Solar Cells", *Imperial College Press, London*, 2003.

[62] C. Zhao, "Interface and Energy Efficiency of Photovoltaics", Ph.D Dissertation, McMaster University, 2013.

[63] W. Dong, G. Jung, S. Kim, and J. Lee, "Effect of ultraviolet-ozone on ITO/P3HT interface for PEDOT:PSS-free polymer solar cells", *Solar Energy Materials and Solar Cells*, 2013, **109**, 240.

[64] S. Alem, J. Gao, and G. Wantz, "Photovoltaic response of symmetric sandwich polymer solar cells with identical electrodes", *Journal of Applied Physics*, 2009, **106**, 044505.

[65] D. Kim, and J. Choi, "Water-Soluble Polythiophene-Single Walled Carbon Nanotube Bulk Heterojunction", *Journal of Nanoscience and Nanotechnology*, 2011, **11**, 8543.

[66] B. Watts, W. Belcher, L. Thomsen, H. Ade, and P. Dastoor, "A Quantitative Study of PCBM Diffusion during Annealing of P3HT:PCBM Blend Films", *Macromolecule*s,

2009, **42**, 8392.

[67] M. Campoy-Quiles, T. Ferenczi, T. Agostinelli, P. Etchegoin, Y. Kim, T. Anthopoulos, P. Stavrinou, D. Bradley, and J. Nelson, "Morphology evolution via self-organization and lateral and vertical diffusion in polymer:fullerene solar cell blends", *Nature Materials*, 2008, **7**, 158.

[68] J. Gao, J. Hui, Y. Hou, and S. Alem, "Planar polymer photovltaic cells with millimeter interelectrode spacing", *Journal of Applied Physics*, 2008, **104**, 084512.

[69] J. Zhao, A. Swinnen, G. Assche, J. Manca, D. Vanderzande, and B. Mele, "Phase Diagram of P3HT/PCBM Blends and Its Implication for the stability for the Stability of Morphology", *Journal of Physical Chemistry B*, 2009, **113**, 1587.